A Far Ultraviolet Spectroscopic Explorer Survey of High Declination Dwarf Novae [1]

Patrick Godon[2], Edward M. Sion

Department of Astronomy and Astrophysics Villanova University, Villanova, PA 19085, patrick.godon@villanova.edu; edward.sion@villanova.edu

Paul E. Barrett

United States Naval Observatory, Washington, DC 20392 barrett.paul@usno.navy.mil

Paula Szkody

Department of Astronomy, University of Washington, Seattle, WA 98195, szkody@astro.washington.edu

ABSTRACT

We present a spectral analysis of the Far Ultraviolet Spectroscopic Explorer (*FUSE*) spectra of eight high-declination dwarf novae (DNs) obtained from a Cycle 7 *FUSE* survey. These DN systems have not been previously studied in the UV and little is known about their white dwarfs (WDs) or accretion disks. We carry out the spectral analysis of the *FUSE* data using synthetic spectra generated with the codes TLUSTY and SYNSPEC. For two faint objects (AQ Men, V433 Ara) we can only assess a lower limit for the WD temperature or mass accretion rate. NSV 10934 was caught in a quiescent state and its spectrum is consistent with a low mass accretion rate disk. For 5 objects (HP Nor, DT Aps, AM Cas, FO Per and ES Dra) we obtain WD temperatures between 34,000K and 40,000K and/or mass accretion rates consistent with intermediate to outburst states. These temperatures reflect the heating of the WD due to on-going accretion and are similar to the temperatures of other DNs observed on the rise to, and in decline from outburst. The WD Temperatures we obtain should therefore be considered as upper limits, and it is likely that during quiescence AM Cas, FO Per and ES Dra are near the average WD T_{eff} for catalcysmic variables above the period gap ($\sim$30,000K), similar to U Gem, SS Aur and RX And.

Subject headings: Accretion, Accretion disks, Stars: white Dwarfs, Stars: dwarf novae

---

[1]Based on observations made with the NASA-CNES-CSA Far Ultraviolet Spectroscopic Explorer. *FUSE* is operated for NASA by the Johns Hopkins University under NASA contract NAS5-32985

[2]Visiting at the Space Telescope Science Institute, Baltimore, MD 21218, godon@stsci.edu

1. Introduction

1.1. Cataclysmic Variables

Cataclysmic variables (CVs) are semi-detached binary systems, in which a white dwarf star (WD) accretes matter from a main-sequence (MS, or post-MS; the *secondary*) star. Accretion takes place via a disk for non-magnetic WDs, and via a column or curtain for magnetic WDs (for a review on CVs see Hack & La Dous (1993); Warner (1995)). The luminosity of a CV can vary significantly, and systems can be found in a state of low luminosity (*quiescence*), high luminosity (*outburst*), or even in a rather *intermediate* state when the system is *active* without reaching its peak luminosity (Robinson 1976; Hack & La Dous 1993; Warner 1995). CVs are divided in sub-classes according to the duration, occurrence and amplitude of their outbursts.

The two main types of CVs are dwarf nova (DN) and nova-like (NL) systems. Dwarf novas are weakly- or non-magnetic disk systems, divided into U Gem systems, SU UMa systems, and Z Cam systems. The U Gem systems are the typical DNs, i.e. those systems exhibiting normal DN outbursts; the SU UMas exhibit both normal DN outbursts, and superoutbursts, which are both longer in duration and higher in luminosity than normal DN outbursts; and the Z Cam systems have standstills where they remain in a semi-outburst state for a long time. Nova-likes form a less homogeneous class, e.g. non-magnetic disk systems found mostly in high state (known anti-DN or VY Scl), systems that exhibit no known low states (UX UMa systems), non-disk magnetic systems (AM Her stars or Polars), magnetic systems with truncated disk (Intermediate Polars), etc. See e.g. Ritter & Kolb (2003) for the classification of CVs .

The binary orbital period in CVs ranges from a fraction of an hour to about a day; however, there is a gap in the orbital period between 2 and 3 hours where almost no CV systems are found (hereafter the "period gap" (Whyte & Eggleton 1980)). U Gem and Z Cam DN systems are found above the period gap, while the SU UMa DN systems are found below the period gap.

1.2. The Standard Model

In the commonly accepted (standard) theory of evolution of CVs, systems evolve through the gap from long periods to shorter periods, driven by angular momentum loss. Above the gap ($P > 3$hrs) magnetic braking (Weber & Davis 1967; Verbunt & Zwaan 1981) is thought to be the dominant mechanism for angular momentum loss due to wind loss of the tidally locked secondary. At about $P \approx 3$hrs, magnetic braking stops when the secondary becomes fully convective, and its radius becomes smaller than the Roche lobe radius: the secondary detaches from the Roche lobe. At this point, gravitational radiation (Faulkner 1971; Paczyński & Sienkiewicz 1981; Rappaport et al. 1982) is believed to take over as the main mechanism for angular momentum loss. The binary separation and period keep on decreasing until $P \approx 2$hrs, at which time the Roche lobe radius becomes again comparable to the radius of the secondary, and the binary becomes again

a contact binary. The disrupted (or *interrupted*) magnetic braking became the standard scenario of CV evolution explaining the presence of the period gap around 3hrs (Paczyński & Sienkiewicz 1983; Rappaport et al. 1983; Spruit & Ritter 1983; Hameury et al. 1988; King 1988; Kolb 1993; Howell et al. 2001).

The first comparison of CV SD temperatures with actual evolutionary tracks (the evolutionary tracks of Mc Dermott & Taam (1989)) was carried out by Sion (1991), who compared the CV WD T_{eff} values as a function of orbital period with the cooling curves of non-accreting WDs and with the theoretical prediction of $\dot{M}$ (hence T_{eff}) versus P of Mc Dermott & Taam (1989). Sion (1991) found some evidence, though far from conclusive, that CV systems evolve across the period gap. However, the standard model is based on an ad-hoc assumption about the mechanism of orbital angular momentum loss, and many of its predictions are in disagreement with the observations (Townsley & Gänsicke 2009). For example, if CVs are evolving from longer period to shorter period across the gap, then short period DNs are older and with a longer history of angular momentum transfer via disk accretion, and their WDs should rotate faster than DN WDs above the gap. However, so far, there is no observational evidence pointing to this. Modifications have been proposed to the standard model (Basri 1987; Hameury et al. 1990; McCormick & Frank 1998; Schenker et al. 1998; Kolb & Baraffe 1999; Clemens et al. 1998; Spruit & Taam 2001; Taam & Spruit 2001; Kolb et al. 2001; King et al. 2002; Taam et al. 2003; Ivanova & Taam 2004). One of the alternatives has even been the suggestion that CVs above and below the gap form two distinct populations not related to each other (Eggleton 1976; Webbink 1981; Andronov N. et al. 2003).

In order to put more constraints on the theories of the evolution of CVs, more observations are needed (Sion 1991; Gänsicke 2004). The standard model gives a prediction of $\dot{M}$ above the period gap (as a function of the binary period) and as a consequence $\dot{M}$ is the most important parameter to test the theory. Unfortunately, to derive $\dot{M}$ from observations proves to be difficult, as it itself relies on many unknowns (e.g. the distance). For example, optical observations seem to indicate that $\dot{M}$ is correlated with the period (Patterson 1984), while FUV spectroscopy (albeit of NLs alone) does not show any correlation at all (Puebla et al. 2007).

1.3. The White Dwarf Temperature: the Case for Dwarf Novae

Recently, Townsley & Bildsten (2003, 2004) have shown that the quiescent effective temperatures T_{eff} of the WD in CVs approaches an equilibrium value when the WD is subject to accretion at an average accretion rate $\dot{M}$ which is constant on time scales similar to the WD core thermal time (∼100Myrs). This equilibrium value is a function of the WD mass and mass accretion rate only. Therefore, knowledge of the quiescent surface temperature of the WD and its mass can be used to obtain an estimate of the average mass accretion rate (it seems counter-intuitive that the effective temperature of the WD would not depends on its age; the limitations and the applications of the relation between $< \dot{M} >$ and T_{eff} are discussed in Townsley & Gänsicke (2009)). As a con-

sequence, CV WD temperature has become the most important observational parameter, together with the binary period and WD mass, to test the theories of the evolution of CVs.

For DNs below the gap, the distribution of WD temperatures obtained from FUV spectroscopic analysis seems to be centered around T_{wd} ∼15,000K, while for systems above the gap the WD temperatures are higher, somewhere between $\sim 30,000$K and up to $\sim 50,000$K (Sion et al. 2008). Above the gap at periods of about 200-300min, the WDs in DNs are about 10,000K cooler than the WDs in VY Scl systems (Godon et al. 2008b). On the other hand, polars (devoid of disks) have the coolest WDs of all, with $T_{wd} < 20,000K$ above the gap and $T < 15,000$K below the gap (Araujo-Betancor et al. 2005) (see Townsley & Gänsicke (2009) for a review WD temperatures in CVs).

Currently, the number of white dwarf temperatures known are as follows. There are 10 NL AM Her systems below the gap and 3 above the gap; 5 NL VY Scl system above the gap; there are 19 DN SU UMa systems below the gap; 12 DN U Gem systems above the gap; and only 2 DN Z Cam systems above the gap. There is a critical shortage in knowledge of the WD effective temperature T_{eff} for DN Z Cam, NL AM Her and NL VY Scl all above the period gap. Thus, detailed comparisons of accreting WDs above and below the gap cannot be made.

However, during quiescence DNs, unlike other CVs, have the advantage of exposing their WD in the FUV for long periods of time. With a temperature range $\sim 12,000 - 50,000$K, the WD peaks in the FUV, and this makes *FUSE* the best instrument to observe the WD of quiescent DNs. Furthermore, DNs offer a fairly reliable estimate of their distances via the absolute magnitude at maximum versus orbital period relation found by Warner (1987) and Harrison et al. (2004). As a consequence, DNs are ideal candidates to observe with *FUSE*, as one can more easily derive the WD temperature.

More precisely, by fitting the observed quiescent spectrum with synthetic spectra, one can, in theory, derive the WD parameters such as the temperature, gravity, rotational velocity, and chemical abundances (mainly for C, N, S, Si). The (instantaneous) mass accretion rate of many systems can be deduced too at given epochs of outburst or quiescence using spectral fitting techniques of FUV spectra. In practice, however, to obtain robust results in the spectral analysis and depending on the quality of the observed spectrum, one needs to know the distance d to the system, the WD mass M_{wd}, and possibly also the inclination of the system (see sections 3 and 4).

For these reasons, we present here a spectroscopic analysis of a sample of dwarf novae from our Cycle 7 *FUSE* survey. The present analysis includes 9 dwarf nova systems: 6 systems above the gap (including 4 Z Cam), 1 below the gap, and 2 with unknown period. The observations are described in the next section, including details of the processing of the spectra and a general description of the lines seen in *FUSE* spectra of DNs. In section 3 we present our synthetic spectral modeling that we use to analyze the spectra. In section 4 we present and discuss the results of the spectral analysis for each system separately. And in the last section we give a short summary of our findings.

2. Observations

2.1. The *FUSE* Spectra

The FUSE targets are listed in Table 1 with their system parameters as follows: column (1) Name, (2) CV subtype, (3) orbital period in days, (4) orbital inclination in degrees, (5) apparent magnitude in outburst, (6) apparent magnitude in quiescence, and (7) priority given as a *FUSE* target (1=high, 2=low).

The observation log is presented in Table 2. The following systems were also listed as targets in our original proposal, but they were not observed with *FUSE*: AD Men, V342 Cen, V1040 Cen, and TZ Per. From the *AAVSO* (American Association of Variable Stars Observers) data (Price 2006), we were able to assess the state of each target at the time of the FUSE observations.

All the *FUSE* spectra were obtained through the 30"x30" LWRS Large Square Aperture in TIME TAG mode. The data were processed with the latest and final version of CalFUSE (v3.2.0; for more details see Dixon et al. (2007)). The *FUSE* data comes in the form of eight spectral segments (SiC1a, SiC1b, SiC2a, SiC2b, LiF1a, LiF1b, LiF2a, and LiF2b) which are combined together to give the final *FUSE* spectrum. To process *FUSE* data, we follow the same procedure we used previously for the analysis of other systems (such as WW Ceti, Godon et al. (2006a)); consequently we give here only a short account of this procedure. The spectral regions covered by the spectral channels overlap, and these overlap regions are then used to renormalize the spectra in the SiC1, LiF2, and SiC2 channels to the flux in the LiF1 channel. We then produced a final spectrum that covers the full *FUSE* wavelength range $905-1187$ Å. The low sensitivity portions of each channel were discarded. In most channels there exists a narrow dark stripe of decreased flux in the spectra running in the dispersion direction, known as the "worm", which can attenuate as much as 50% of the incident light in the affected portions of the spectrum; - this is due to shadows thrown by the wires on the grid above the detector. In the present observations, the worm affected mainly the 1bLiF channel. Because of the temporal changes in the strength and position of the "worm", CALFUSE cannot correct target fluxes for its presence. Therefore, we carried out a visual inspection of the *FUSE* channels to locate the worm and we *manually* discarded the portion of the spectrum affected by the worm. We combined the individual exposures and channels to create a time-averaged spectrum weighting the flux by the exposure time and sensitivity of the input exposure and channel of origin.

For all the targets we had to remove the edges of the SiC channels and the worm (∼1140-1180Å) in the 1bLiF channel. In some cases we had to remove entire channels due to their very poor S/N. Specifically, we proceeded as follows:
- AQ Men, we kept only the 2aLif and 2bLif channels;
- HP Nor, we removed all the SiC channels while keeping the LiF channels;
- DT Aps, we removed large portions (at the edges) of the SiC channels;
- AM Cas, we discarded the 2bLiF, 2bSiC, 2aLiF and 2aSic channels and only used 1aSiC, 1bSiC,

1aLiF, and 1bLiF;
- NSV 10934, we removed 1aSic, 2bSiC, 2bLiF;
- FO Per, we kept all the channels;
- ES Dra, we kept all the channels; and
- V433 Ara, all the SiC channels were discarded and only the LiF channels were kept.

2.2. The *FUSE* Lines

The main emitting components contributing to the *FUSE* spectra of DNs are the accretion disk and the WD: the disk dominates during outburst, while the WD dominates during quiescence. The main feature of the spectra is the broad Lyβ absorption feature, which can easily be used to assess the gravity and temperature of the emitting gas. At higher temperatures, as the continuum rises in the shorter wavelengths, the higher orders of the Lyman series also become visible; however, they become narrower.

Additional broad absorption lines of metals (C, S, Si, ..) are detected and help determine the chemical abundances and projected rotational velocity of the emitting gas. In the present spectra, the main absorption features observed are: C II (1010 Å), C III (1175 Å), Si III (≈1108-1114 Å and ≈1140-1144 Å), Si IV (≈1067 Å and ≈1120-1130 Å), S IV (1073 Å), and N II (1085 Å when not contaminated by air glow).

On top of the spectrum, broad emission lines are also found in two of the systems, NSV 10934 and AQ Men, mainly the O VI doublet and C III (977Å and 1175 Å). The broad emission lines in NSV 10934 and AQ Men originate from the hot accretion region on the white dwarf, and possibly also from the inner disk itself, as expected for high-inclination DNs in quiescence such as BZ UMa (Gänsicke et al. 2003) or EK TrA (Godon et al. 2008a). AQ Men is eclipsing and the presence of broad emission lines in NSV 10934 might be an indication that it is a high inclination system.

All our *FUSE* spectra show some ISM molecular hydrogen absorption. The most affected targets reveal a spectrum "sliced" at almost equal intervals (∼12Å); starting at wavelengths around 1110Å and continuing towards shorter wavelengths all the way down to the hydrogen cut-off around 915Å . In the affected *FUSE* spectra, we identified the most prominent molecular hydrogen absorption lines by their band (Werner or Lyman), upper vibrational level (1-16), and rotational transition (R, P, or Q) with lower rotational state (J=1,2,3).

In addition, the targets that are weak *FUSE* sources exhibit sharp emission lines from air glow (geo- and helio-coronal in origin; some of which is due to sunlight reflected inside the telescope), such as H I series, S VI (934, 944), O VI doublet, C III (977), and He I (1168).

For each system, we mark on the figures the lines that are detected as well as lines that are commonly seen for comparison. The lines that are commonly seen in the *FUSE* spectra of quiescent

DN systems are as follows. At lower temperatures ($15,000\text{K} < T < 25,000\text{K}$), the observed lines are (e.g. Godon et al. (2008a)) C III (1175 Å), C II (1066 Å), Si III (≈1108-1114 Å and ≈1140-1144 Å), and N II (1085 Å when not contaminated by air glow). At higher temperatures (T> 25,000K), as the continuum rises in the shorter wavelengths, the higher orders of the Lyman series are revealed. At these temperatures the S IV (1073 Å) absorption line starts to appear, and, as there is more flux in the shorter wavelengths, the C II (1010 Å) absorption line also becomes visible (e.g. Urban & Sion (2006); Long & Gilliland (1999)). At still higher temperature (T> 50,000K), the C II and Si III lines disappear, and the spectrum becomes dominated by high order ionization lines such as N IV (≈923 Å), S VI (933.5 & 944.5 Å), S IV (1063 & 1073 Å), Si IV (1066.6 Å), and O IV (1067.8 Å) (see e.g. Hartley et al. (2005); Sion et al. (2007)).

Because of the low quality of the spectra, the observed wavelengths cannot be determined accurately and, therefore, we do not list the wavelengths of the lines in a table. The lines are discussed for each object separately.

3. Spectral Modeling

3.1. The Synthetic Stellar Spectral Codes

Before we carry out the actual fit for each individual observed spectrum, we create a grid of model spectra for high-gravity stellar atmospheres using codes TLUSTY and SYNSPEC[1] (Hubeny 1988; Hubeny & Lanz 1995). Atmospheric structure is computed (using TLUSTY) assuming a H-He LTE atmosphere; the other species are added in the spectrum synthesis stage using SYNSPEC. For hot models (say $T > 50,000\text{K}$) we switch the approximate NLTE treatment option in SYNSPEC (this allows us to consider and approximate NLTE treatment even for LTE models generated by TLUSTY). We generate photospheric models with effective temperatures ranging from 12,000K to 75,000K in increments of about 10 percent (e.g. 1,000K for T≈15,000K and 5,000K for T≈70,000K). As the WD mass in these DN systems is not known, we choose values of $Log(g)$ ranging between 7.5 and 9.5. We also vary the stellar rotational velocity $V_{rot}sin(i)$ from 100km s^{-1} to 1000km s^{-1} in steps of 100km s^{-1}. As a default, solar abundances are assumed for all the models in the grid. We have, however, the option to vary the chemical abundances of individual elements in the models in the grid. For any WD mass, there is a corresponding radius, or equivalently, one single value of $Log(g)$ (e.g. see the mass radius relation from Hamada & Salpeter (1961) or see Wood (1995); Panei et al. (2000) for different composition and non-zero temperature WDs).

The same suite of code is also used to generate spectra of accretion disks (Wade & Hubeny 1998) based on the standard model of Shakura & Sunyaev (1973). In the present work we use disk spectra from the grid of spectra generated by Wade & Hubeny (1998) as well as disk spectra

[1] http://nova.astro.umd.edu; TLUSTY version 200, SYNSPEC version 48

that we generate. A detailed description of the procedure to generate such disk spectra is given in Wade & Hubeny (1998).

3.2. Synthetic Spectral Model Fitting

Before carrying out a synthetic spectral fit of the spectra, we masked portions of the spectra with strong emission lines, strong ISM molecular absorption lines, detector noise and air glow. These regions of the spectra are somewhat different for each object and are not included in the fitting. The regions excluded from the fit are in blue in the figures. The excluded ISM quasi-molecular absorption lines are marked with vertical labels in the figures.

After having generated grids of models for each target, we use FIT (Press et al. 1992), a χ^2 minimization routine, to compute the reduced χ^2_ν (χ^2 per number of degrees of freedom) and scale factor values for each model fit. While we use a χ^2 minimization technique, we do not blindly select the least χ^2 models, but we examine the models that best fit some of the features such as absorption lines (see the fit to the *FUSE* spectrum alone) and, when possible, the slope of the wings of the broad Lyman absorption features. When possible, we also select the models that are in agreement with the distance of the system (or its best estimate).

The flux level at 1000Å (between Lyδ and Lyγ) is close to zero for temperatures below 18,000K, at 30,000K it is about 50% of the continuum level at 1100Å and it reaches 100% for T>45,000K. At higher temperature (T>50,000K) the spectrum becomes pretty flat and there is not much difference in the shape of the spectrum between (say) a 50,000K and a 80,000K model. When fitting the shape of the spectrum in such a manner, an accuracy of about 500-1,000K is obtained, due to the S/N. In theory, a fine tuning of the temperature (say to an accuracy of about ±50K) can be carried out by fitting the flux levels such that the distance to the system (if known) is matched. However, the fitting to the distance depends strongly on the radius (and therefore the mass) of the WD. In all the systems presented here the mass of the WD and the distance are unknown and therefore we are unable to assess the temperature accurately. Furthermore, since the Lyβ profile depends on both the temperature and gravity of the WD, the accuracy of the solution is further decreased as there is a degeneracy in the solution, namely the solution spreads over a region of the $Log(g)$ and T parameter space. And last, reddening values are rarely known, therefore increasing even more the inaccuracy of assessing the temperature by scaling the synthetic flux to the observed flux. As a consequence, for each target we present more than one model fit.

For DT Aps and ES Dra we vary the abundances; however, because of the low S/N, for all the other spectra we fit solar abundance models and do not change the abundance of the species.

The WD rotation ($V_{rot}sin(i)$) rate is determined by fitting the observed *FUSE* spectrum with WD models with increasing values of the rotational velocity. We did not carry out separate fits to individual lines but rather tried to fit the lines and continuum in the same fit.

For each spectrum, when possible, we try to fit a single WD model, a single disk model, and a composite WD+disk model, assuming different reddening values. For all the systems presented here the WD mass is unknown and the distance is estimated using the maximum magnitude/period relation (Warner 1987; Harrison et al. 2004), or (when the period is unknown) the method described by Knigge (2006, 2007) (see Table 3).

For the single WD model, we vary the temperature while first keeping the WD mass constant, starting at about $0.4M_{\odot}$. Once the lowest χ^2 has been found for a given mass, we vary the projected rotational velocity, and possibly also the abundances, to further lower the χ^2 and obtain a best fit. Once the best fit has been found for that mass, we assume a slightly larger mass and again vary the temperature until the lowest χ^2 is found. We follow this procedure iteratively until we reach a mass of about $1.2M_{\odot}$. The next step is to find, from all these lowest χ^2 models, which one agrees best with the distance estimate, or which one has the lowest χ^2 of all (if the constraint on the distance cannot be used). For the single disk model, we carry out a similar procedure by varying the mass accretion rate and inclination assuming discrete values of the WD mass, and then chose the least χ^2 model agreeing best with the distance. And last, we use the same procedure for the WD+disk composite modeling to find the best fit model.

4. Results and Discussion

Four systems were caught in deep quiescence, and their *FUSE* spectra have such a low S/N that they are unusable. This is due not only to the intrinsic low brightness of the targets, but also to the loss of data in some *FUSE* channels (mainly SiC) and to the loss of good exposure time (due e.g. to jitters). These four systems are VW Tucanae/HV 6327, IK Normae, V663 Arae/S 5893, and V499 Arae/S 6115. The remaining eight systems that were successfully observed are presented here.

4.1. Southern Hemisphere Systems

4.1.1. HP Normae/HV 8865

HP Nor is a DN Z Cam system (Vogt & Bateson 1982) which exhibits coherent oscillations during outbursts with a period $\sim$ 18.6s (Pretorius et al. 2006). Its magnitude varies between V=12.6 at maximum and V=16.4 at minimum (Bruch & Engel 1994). The distance to HP is not known, and since its period is also unknown, we have no way to assess its distance. HP Nor was observed with *FUSE* on April 13 (JD 2454203.7). Data from the AAVSO and AVSON imply that the system was in a low state of brightness $V \sim 15$, though it did not reach its lowest magnitude $V = 16.4$. The continuum flux level of the *FUSE* spectrum is roughly consistent with the continuum flux level in the optical around 3,200Å obtained by Munari & Zwitter (1998),

who observed the system in an apparent decline from outburst with V=14.18 and a flux level of 2×10^{-14}ergs cm^{-2}sec^{-1}Å^{-1}. The *FUSE* spectrum of HP Nor is presented in Figure 1. The reddening toward HP Nor is not known, however the Galactic reddening in this direction is 0.63. Therefore, in the following we model HP Nor assuming both E(B-V)=0.0 and E(B-V)=0.2 .

E(B-V)=0.0 For the single WD model, assuming $M_{wd} = 0.8M_{\odot}$, we find a temperature of 37,000K and a distance of 648pc. The projected rotational velocity is $v_{rot} \sin i = 1000$km/s to fit the C III (1175) line profile. The χ^2 obtained is smaller than one due to the poor S/N, namely $\chi^2_{\nu} = 0.107$. The results are listed in Table 4, where we also present a $0.4M_{\odot}$ WD and a $1.2M_{\odot}$ WD models. For the single disk models, assuming a $0.8M_{\odot}$ WD mass, we find $\dot{M} = 10^{-9.0} M_{\odot}$/yr, $i < 41°$, d=1603pc and $\chi^2_{\nu} = 0.104$. Again, in Table 4 we list the results assuming different values for M_{wd}. There is basically no difference in the quality of the fit between the disk model and the single WD model. A WD+disk composite model does not improve the fit. Because the WD mass and the distance are unknown, we are left with solutions spanning a large area in the parameter space, especially for the composite WD+disk models. We do not list the results for the composite models as there is clearly a degeneracy in the solution.

E(B-V)=0.2 Dereddening the spectrum for E(B-V)=0.2 increases the temperature of the single WD model by 3,000K and reduces the distance by a factor of 2. The χ^2 obtained is slightly lower $\chi^2_{\nu} \approx 0.096$. For the single disk models, the mass accretion rate obtained is larger by a factor of up to ~ 30, while the distance is reduced by about half (all the models are listed in Table 4). Again, there is not much difference between the single disk model and the single WD model. The WD+disk composite models again do not bring any improvement in the fit, rather the opposite.

It is most likely that the spectrum is due solely to the heated WD as the system was observed in a relatively low state. The best disk models reach a mass accretion rate that is too large for such a low state. Our preferred model is the single WD model for E(B-V)=0.2, assuming an intermediate mass of $0.8M_{\odot}$ with $T = 43,000$K. This model is shown in Figure 2.

4.1.2. AQ Mensae/EC 05114-7955

AQ Men (also known as EC 05114-7955 (Cheng et al. 2001)) has a magnitude around 14-15, but no outburst has been detected so far. Its period is 0.141466d (Patterson 2002). Its optical spectrum suggests it is a DN, however, the possibility that it is a NL cannot be ruled out (Cheng et al. 2001). Cheng et al. (2001) classified it as an *unusual/peculiar* CV, that shows large-amplitude flickering and a low-excitation spectrum, where the C III/N IIIλ4650Å blend is also seen in emission, and suggested that the double peak in the line profiles might indicate that it is a highly inclined system. Patterson (2002) showed that it is actually an eclipsing system with superhumps and a precession period of 3.77±0.05d.

A *FUSE* spectrum of AQ Men was obtained on 22 November 2006, at which time we only know it was at a magnitude between 14 and 15 (AAVSO data). For the modeling, we do not know *a priori* whether the disk or the WD dominates the FUV spectrum. In spite of its very low continuum flux level (at most $\sim 1 \times 10^{-14}$ergs cm^{-2}sec^{-1}Å^{-1}; see Figure 3) the spectrum (binned at 0.2Å) exhibits features that are easily identified such as the molecular hydrogen absorption lines, some Si III & Si IV and C III absorption features, as well as broad emission from the O VI doublet and the C III (1175) multiplet. The emission is consistent with DNs observed in quiescence, and the large (rotational) broadening of the C III emission (>6Å, or $v > 1,000$km/s) agrees with the fact that it is highly inclined. However, broad emission lines are often observed in nova-likes systems too. In the present case the *FUSE* spectrum of AQ Men is more similar to that of a quiescent DN such as EK TrA (Godon et al. 2008a), as the emission lines are not as strong as those exhibited by nova-like systems (such as AE Aqr; see the *MAST* archive).

The distance to AQ Men (using the relations of (Warner 1987; Harrison et al. 2004);see Table 3) is possibly $d \approx 710$pc. AQ Men has no known reddening but the Galactic reddening in its direction is $E(B-V) = 0.18$. We model its *FUSE* spectrum first assuming no reddening, and then assuming $E(B-V) = 0.10$. Since it is apparently an eclipsing system (Patterson 2002) we set the inclination angle to $i = 81°$. The spectrum of AQ Men is so poor, that we only try to fit the flux level in order to obtain the distance to the system irrelevant of the value of the χ^2. Since we only fit the flux level, we do not show any figure of the results.

Single Disk Model. For the single disk model fit, we find that, in order to fit the distance, the mass accretion rate has to be $\dot{M} = 10^{-9.5} M_{\odot}$yr^{-1} assuming a WD mass of $1.2M_{\odot}$; and it increases to $\dot{M} = 10^{-8.75} M_{\odot}$yr^{-1} for $M_{wd} = 0.35M_{\odot}$ Next, we carried the same model fits but we deredden the spectrum assuming $E(B-V) = 0.1$. We obtain larger mass accretion rates as listed in Table 4. From these single disk models, we note that if the emission is due to a disk, then its accretion rate is consistent with the outburst state of a DN, where the minimum value obtained ($\dot{M} = 10^{-9.5} M_{\odot}$yr^{-1}) is for the larger mass ($1.2M_{\odot}$) assuming no reddening. This is the lower limit of $\dot{M}$ for all reasonable values of M_{wd} ($\leq 1.2M_{\odot}$) and $E(B-V) \geq 0.0$.

Single WD Model. Assuming no reddening and for a mass $M = 0.4M_{wd}$, we fit the flux with $T = 24,000$K. Increasing the mass decreases the radius and therefore the flux is fit with a larger temperature reaching 36,000K for a $1.1M_{\odot}$ WD. Dereddening the spectrum assuming $E(B-V) = 0.10$, we obtain higher temperatures, with $T = 60,000$K for $M = 1.1M_{\odot}$. From the single WD modeling we obtain that if the spectrum is due to the WD alone, then its temperature must be $T \geq 24,000$K and it increases with increasing mass and reddening. This is therefore the lower limit for the WD temperature of AQ Men, assuming it spectrum is solely from the WD. Since there is no additional constraints on the parameters of the system, we are unable to carry out a multi-component (WD+Disk) model fit as there is degeneracy. However, we note that, because of its inclination (Patterson 2002), the disk masks the WD, except if it is in a quiescent-like state.

For AQ Men we can summarize these results as follows. If the system is a DN, then it is probably in a lower state, where the WD dominates the FUV and has a temperature of at least 24,000K. The disk models do not agree with a quiescent mass accretion rate for DN. If the system is a NL, then the disk is in outburst and dominates the FUV with a mass accretion rate $\dot{M} \leq 3 \times 10^{-10} M_{\odot} \mathrm{yr}^{-1}$, barely larger than $\dot{M}_{critic}$ but consistent with the theory.

4.1.3. V433 Arae/S 6006

V433 Ara is an eclipsing Z Cam DN system, with a period of 4.698h (Woudt et al. 2005). From the AAVSO data, we find that the system was in quiescence at the time of the *FUSE* observations, on 18 Feb 2007. However, its exact magnitude during the *FUSE* observations is not known. The *FUSE* spectrum of V433 Ara (Figure 4) is the poorest spectrum of all the observed spectra we model, it consists only of the LiF channels, and consequently we are not able to model it properly. We model only the flux level to obtain some constraints on the temperature and mass of the WD and possibly on the mass accretion rate. The galactic reddening in the direction of V433 Ara is about 0.2 but the actual reddening of V433 Ara is not known. We assume here E(B-V)=0.0 and 0.1. Also from the period-luminosity relation we find a distance of ∼1200pc. Since the system was not observed in outburst the spectrum could be either that of quiescence (∼18mag) with the WD dominating the spectrum, or standstill (∼16.5mag) at an intermediate level (Woudt et al. 2005) where the inflated disk dominates the spectrum (because of the high inclination). We model the spectrum with single disk and single WD models, fixing d=1200pc and $i \sim 80°$. Since the spectrum is of such poor quality (see Figure 4) we do not show the model, as we only fit the *level of the continuum* (i.e. there are no features to match).

Single Disk Models. The main results for the disk model are presented in Table 4. For a larger WD mass the mass accretion needed to fit the spectrum decreases. If the system was observed with *FUSE* in a standstill, then the mass accretion rate should rather be on the lower side in agreement with a large WD mass and little reddening. However, because of the large distance, the reddening might not be negligible and we therefore suspect that V433 Ara could have been observed in quiescence and that its FUV flux might be due to a WD rather than a disk.

Single WD Models. The WD models are listed in Table 4. The main result is that the temperature of the WD increases with the mass of the WD and the reddening. From these, it appears that the lower limit for the WD temperature of V433 Ara is 24,000K. Again, if the reddening is not negligible (E(B-V)=0.1 or larger), then the WD mass has an upper limit of about $0.8 - 1.0 M_{\odot}$, as it is very unlikely that the WD has a temperature $T \sim 75,000$K (most DNs's WDs have $T < 50,000$K).

4.1.4. DT Apodis/S 5646

DT Aps was first identified as a DN by Vogt & Bateson (1982), and it is classified as a SS Cyg sub-type (Downes et al. 2001). Apart from that little is known about this high declination southern dwarf nova.

DT Aps was observed with *FUSE* on 28 April 2006 and on 3 May 2006. These observation were taken 4 and 9 days (respectively) after an outburst recorded by the AAVSO on 24 April 2006. It is not known how long the outburst lasted, but it is likely that the first observation caught the system while it was still in a relatively active state. The second observation was taken after the system had more time to decline to quiescence, however, it was 10 times shorter than the first one and it is therefore unusable. Even though the first observation lasted basically 70ks, the SiC channels were very noisy and large portions of the spectral segments had to be discarded. The *FUSE* spectrum of DT Aps is shown in Figure 5.

In the shorter wavelengths (upper panel) the spectrum consists mainly of sharp air glow emission lines (noise) with some possible C III (λ977) emission; at longer wavelengths (middle panel) the spectrum reveals a prominent broad and deep Lyβ absorption feature, which is the main feature of the spectrum. In the longer wavelengths (lower panel) the silicon absorption features Si III & Si IV (around $\lambda \sim 1110 - 1130$Å) are very deep and could possibly indicate a high silicon abundance. However, since the other silicon absorption features are not as pronounced, it is likely that the deep silicon features are due to incorrect background subtraction. Alternatively, there could be some emitting components contributing some flux around $\lambda \sim 1150 - 1160$Å . The C III (λ1175) absorption multiplet is also rather deep and broad, possibly due to a large velocity broadening. The spectrum is rather noisy and of poor quality, making it difficult to model.

Since the period of the system is not known, we have no way to estimate its distance. The reddening of the source is also not known but the galactic reddening in its direction is $E(B-V) = 0.09$. A reddening of 0.05 will not affect the results by much and therefore, in order to assess the effect of the reddening on the results, we carry out model fits assuming both $E(B-V) = 0.0$ and $E(B-V) = 0.09$. Since the system was observed 4 days after an outburst, the flux is either due to a disk (with a lower accretion rate than the peak outburst), a heated WD or both.

Single Disk Models. For a $0.35M_{\odot}$ WD, the best disk model has $\dot{M} = 10^{-8.5} M_{\odot}\mathrm{yr}^{-1}$, $i = 18°$, d=4450pc and $\chi^2 = 0.2127$. As we increase the WD mass, the mass accretion rate needed to fit the spectrum decreases and for a $1.2M_{\odot}$ WD, the best disk model has $\dot{M} = 10^{-10} M_{\odot}\mathrm{yr}^{-1}$, $i = 18°$, d=2800pc and $\chi^2 = 0.2138$. The difference in the χ^2 value between these best fit models is not significant and we have therefore no way to find out the mass of the WD from these fits. We note that since the system was observed *after* an outburst, it is clear that its mass accretion rate is much lower than at outburst, consistent with the higher WD mass and smaller distance. Next, we deredden the spectrum assuming $E(B-V) = 0.09$ and carry out the same procedure (since the distance we obtained is so large, it is likely that the spectrum is affected by reddening). We find a

slightly larger mass accretion rate (with about the same distance) and a χ^2 value larger by about 5-10%. The smaller mass accretion rate is obtained for the $1.2M_{\odot}$ WD, with $\dot{M} = 10^{-9.5} M_{\odot}\mathrm{yr}^{-1}$, $i = 18°$, d=2950pc and $\chi^2 = 0.2273$. None of the disk models provided an adequate fit to the spectrum as the deep and broad absorption feature around 1130Å and the 'hump' feature around 1160Å could not be fit.

Single WD Models. The lowest mass model ($M = 0.4M_{\odot}$) gives a temperature of 34,000K, a distance of ∼3000pc and $\chi^2 = 0.2115$; while the largest mass model ($M = 1.2M_{\odot}$) gives a temperature of 40,000K, a distance of ∼1000pc and $\chi^2 = 0.2125$. These models do not provide a better fit than the single disk models. We then ran an intermediate mass model ($M = 0.8M_{\odot}$) with an increased silicon abundance and found that the fit could be slightly improved when $Si > 10\times$ solar. That best fit model has T=37,000K, d=1700pc and $\chi^2 = 0.2050$ (see Figure 6). In order to fit the C III (λ1175) line profile all these models have a rotational velocity of about 500km/s. Here too we check how a reddening of $E(B-V) = 0.09$ affects the results and we find no improvement, rather the opposite, the χ^2 is larger by about 5-10%. The smallest distance is obtained for the $M = 1.2M_{\odot}$ model, with $T \sim 42,000$K, d=624pc and $\chi^2 = 0.2290$.

Lastly, we tried composite WD+disk models but they did not improve the fit, and because of the unknown mass, distance, and inclination the results for the composite models were inconclusive.

4.1.5. NSV 10934/Oct

NSV10934 is a SU UMa sub-type dwarf nova (Kato et al. 2002, 2004; Downes et al. 2001). It shows superoutbursts (Kato et al. 2004) during which superhumps are detected with a period of 0.07478d. Shorter (normal) outbursts occur at intervals of about 40-60 d. However, due to the unusual rapid fading of its normal outbursts, Kato et al. (2004) note that it may be an intermediate polar (IP) candidate showing SU UMa properties.

NSV 10934 was observed with *FUSE* on 28 June 2006 (JD2453914.6), and on 30 June 2006 (JD2453916.7), 28 days (or possibly less) after the end of an outburst lasting a week. At the time of the *FUSE* observation, the system was in quiescence. The *FUSE* spectrum of NSV 10934 consists of 5 orbits from the first data set and 4 orbits form the second data set combined together (Figure 7). The system was possibly at a magnitude $\sim 15.5 - 16.0$. The flux level of the spectrum is pretty low and the *FUSE* spectrum suffers from a very low S/N. In spite of that we see that there is a rather flat continuum with very broad emission lines from C III (λ977 & λ1175) and the O VI doublet. The broad emission lines are an indication that the system is viewed at a high inclination angle, possibly $i \geq 60°$ (see e.g. the broad emission lines of the DN EK TrA, with $i = 60°$, in quiescence (Godon et al. 2008a)). Since eclipses have not been detected, we can assume $i < 80°$. The Lyβ broad absorption feature is not detected, possibly due to the left wing of the very broad oxygen emission feature. However, in that respect, the continuum is *a priori* more characteristic of

an accretion disk seen at a high inclination angle. Therefore, in the following we model the *FUSE* spectrum of NSV 10934 with a single WD, a single disk and a WD+disk. We also assume two reddening values, E(B-V)=0 and E(B-V)=0.1 to assess how reddening affects the results. Using the period-luminosity relation we find that the distance to the system is possibly $d \sim 150$pc (see Table 3).

WD models. Since NSV 10934 was observed in quiescence and has been classified as a DN, we decided to model its *FUSE* spectrum first with a single WD. For any WD mass between 0.4 to $1.2M_{\odot}$ there is no synthetic spectrum that can fit the observed spectrum and the distance at the same time. In order to fit the flux between 1000Å and 1080Å the temperature of the WD has to be of the order of 25,000K and higher (depending on the mass) and this leads to a distance well above 200pc. WD models that lead to a distance of about 200pc have a lower temperature and do not fit the continuum of the spectrum at all. We then decided to deredden the observed spectrum assuming E(B-V)=0.1 to see if this improves the modeling and the best model obtained in this case is for a $1.2M_{\odot}$ WD with a temperature of 30,000K. This WD model gives a distance of 216pc and $\chi^2 = 0.232$ and it is barely better than the WD models obtained without dereddening the spectrum. We remark here that the worst models obtained are for the lower WD masses.

Disk Models. Since the WD models are less than satisfactory, we decided to run single disk models, first assuming E(B-V)=0.0. For $M_{wd} = 0.4M_{\odot}$ the mass accretion rate needed to fit the spectrum is too large for quiescence and gives a distance far too large. For $M_{wd} = 0.8M_{\odot}$ the best fit model has $\dot{M} = 10^{-10}M_{\odot}\mathrm{yr}^{-1}$ and $i = 75°$, and gives a distance of 185pc and $\chi^2 = 0.196$. The best fit model, however, is obtained for the largest mass in the run with with $M_{wd} = 1.2M_{\odot}$, $\dot{M} = 10^{-10.5}M_{\odot}\mathrm{yr}^{-1}$ and $i = 81°$, and gives a distance of 144pc and $\chi^2 = 0.160$ (all shown in Table 4). Next we dereddened the spectrum assuming E(B-V)=0.1, the best fit model is for $M_{wd} = 1.2M_{\odot}$ with $\dot{M} = 10^{-10}M_{\odot}\mathrm{yr}^{-1}$ and $i = 81°$, which gives a distance of 187pc and $\chi^2 = 0.146$. This best disk model is shown in Figure 8. All the models are listed in Table 4.

At this stage, we tried to add a WD spectral component to the synthetic disk spectrum but it did not improve the fit. We note that with this inclination the WD might not be visible even with a low mass accretion rate, as the outer part of the disk might be masking it. The high inclination is also in agreement with the large broadening of the carbon and oxygen emission features.

4.2. Northern Hemisphere Systems

4.2.1. AM Cassiopeiae/258.1928

Because of its short period activity and relatively high brightness (mag 12.3-15.2 (Downes et al. 2001)) AM Cas was discovered long ago by Hoffmeister (1929). Its relation to dwarf novae was

suggested by Richter (1961), who observed a 9 days outburst cycle and the occurrence of standstills. It was classified as a Z Camelopardalis system by Notni & Richter (1984). Optical spectra were later obtained by Richter et al. (1988) and confirmed the classification of AM Cas as a Z Cam DN as well as its short (mean) outburst cycle period (8.2 days). The orbital period of the binary system is 0.165 d (=3.96 hr) as reported by Taylor & Thorstensen (1996), who also obtained 3 optical spectra $\sim 4500 - 6300$Å. One of the spectra is in quiescence with a flux $< 10^{-15}$ergs s^{-1}cm^{-2}Å^{-1}, and the two other spectra are in an intermediate state with a maximum flux reaching $\sim 10^{-14}$ergs s^{-1}cm^{-2}Å^{-1} at 4500Å and decreasing toward longer wavelengths.

AM Cas was observed with *FUSE* on 19 October 2006 (JD 2454027.1) and the AAVSO data indicated it was in standstill at that time with a visual magnitude of 13.8 (the system can reach 12.3 mag). The *FUSE* spectrum has a continuum flux level reaching 1.5×10^{-13}ergs s^{-1}cm^{-2}Å^{-1} (Figure 9), which makes AM Cas the brightest FUV target we observed.

The *FUSE* data for AM Cas consist of 6 exposures (i.e. orbits). The quality of the spectrum is relatively good and reveals some moderate ISM molecular hydrogen absorption lines. The C III (1175) line might be blue-shifted by 3Å, however this is the region affected by the worm and the feature might be an artifact of the worm rather than a true absorption feature. In the short wavelengths (< 950Å) the flux does not go to zero and the continuum there is about 1/3 of the flux at longer wavelengths (> 1000Å), indicative of a high temperature. On the other side, the Lyβ is rather deep and wide indicative of a lower temperature. It is possible that the flux in the shorter wavelengths is due to broad emission lines from N IV ($\sim \lambda 923$), S VI ($\lambda\lambda 935, 945$), similar to the broad feature around 976Å- 980Å due to C III ($\lambda 977$) and N III ($\lambda 980$). However, there is no sign of emission from the O VI doublet. Another possibility is that of two emitting components (disk+WD), one contributing relatively more flux in the shorter wavelengths, and the other having a deep Lyβ profile. Since we known AM Cas was observed in an intermediate (standstill) state we may expect both the WD and the disk to contribute to the flux. For the modeling we assess a distance of 350pc using the period-luminosity relation (see Table 3). The reddening of AM Cas is not known, however, the Galactic reddening in its direction is pretty large (~ 0.9) and it is therefore possible that AM Cas itself has a significant reddening. For this reason, we model the FUSE spectrum of AM Cas assuming no reddening and assuming a reddening of 0.2, as this allows us to assess how the reddening affects the results. We first ran models assuming E(B-V)=0.0.

Single Disk Models. The single disk models are unable to fit the deep Lyβ feature and the flux in the shorter wavelengths at the same time. The best models (least χ^2, and consistent with the distance and outburst state) are as follows. For a WD mass $M_{wd} = 0.4M_{\odot}$, $\dot{M} = 10^{-8.5}M_{\odot}$yr^{-1}, $i \approx 60^{\circ}$, d=324pc and $\chi^2 = 0.611$; as the mass increases to $M_{wd} = 0.8M_{\odot}$, we get $\dot{M} = 10^{-9.5}M_{\odot}$yr^{-1}, $i \approx 20^{\circ}$, d=376pc and $\chi^2 = 0.614$. From the single disk models alone we infer that the mass of the WD must be $M_{wd} \leq 0.8M_{\odot}$, the system must have an inclination $i \leq 60^{\circ}$ and the mass accretion rate in outburst is $\dot{M} = 10^{-9.5} - 10^{-8.5}M_{\odot}$yr^{-1}.

Single WD Models. The best fit model was obtained for a $0.4M_{\odot}$ WD with a temperature of 30,000K, a projected rotational velocity of 1000km/sec, a distance of 307pc, and $\chi^2 = 0.623$. Models with a larger mass (and consequently a smaller radius) gave an even smaller distance. The single WD model indicates, as the single disk model, a rather small mass and an intermediate temperature.

Composite WD+Disk Models. For the composite WD plus disk models we initially chose an average WD mass of $0.8M_{\odot}$. We find that the least χ^2 model is for a mass accretion of $2 \times 10^{-10} M_{\odot}$/yr, an inclination $i = 18°$, a WD temperature $T = 36,000$K with a projected rotational velocity $V_{rot} \sin i$=500km/s. This gives a distance of 373pc, $\chi^2 = 0.563$, with the WD contributing 41% of the flux and the disk 59%. This model, though better than the single WD and single disk models, also does not fit too well the high flux in the lower wavelengths. This model is shown in Figure 10. In order to fit the lower wavelength region of the spectrum we have to increase the temperature of the WD to about 40,000K. This in turn increases the distance to $d > 400$pc and $\chi^2 > 0.57$. We note that performing the same WD+disk composite model fit with a lower mass gave about the same results but with a larger distance, while a larger mass gave a smaller distance. However, we do not consider these models here as we used a distance in agreement with the distance obtained using the period-mangitude relations of Warner (1987) and Harrison et al. (2004), namely $d \approx 350$pc (see Table 3).

E(B-V)=0.2 We performed the same model fits. The best fit model is a WD+disk composite model with $M = 0.55M_{\odot}$, $\dot{M} = 3 \times 10^{-9} M_{\odot}$/yr, an inclination $i = 18°$, a WD temperature $T = 35,000$K with a projected rotational velocity $V_{rot} \sin i$=400km/s. The distance obtained is 331pc, $\chi^2 = 0.538$, with the WD contributing only 11% of the flux and the disk 89% (Figure 11). This model does better at fitting the spectrum both at the shorter and longer wavelengths. However, it fits the Lyβ region a little less well. The higher mass models do not perform as well and give a distance $d < 250$pc.

4.2.2. FO Persei/22.1939

FO Per has a mean outburst cycle of about 10 days (Howarth 1976; Gessner 1978) and belongs to those DN with a particularly high outburst rate. Its magnitude varies between 11.8 and 16.2 (Downes et al. 2001). It was observed in the optical by Bruch et al. (1987); Bruch (1989) but these and more recent observations have not been able to unambiguously determine the orbital period of the system: it is not clear whether the period is 3.52h or 4.13h (Sheets et al. 2007). However, with these values we assess the distance to FO Per using the absolute outburst magnitude/Period relation (Warner 1987; Harrison et al. 2004) (see Table 3) and we obtain $d \approx$ 270pc.

FO Per was observed with *FUSE* on 11 Feb 2007 (JD2454142.1) and the AAVSO data indicate it was caught in an intermediate state of brightness at 13.4 mag. The *FUSE* spectrum of FO Per is of moderately good quality exhibiting both interstellar (molecular hydrogen) and intrinsic absorption features (see Figure 12). There is definitely more flux in the longer wavelengths: this is a sign of either a strong reddening or a moderate temperature. Except for air glow, there are no emission lines.

Even though FO Per was caught with *FUSE* while reaching 13.4 mag (brighter than AM Cas at 13.8 mag), it has a continuum FUV flux level 3 times lower than that of AM Cas: namely, at the time of the observations FO Per was *redder* than AM Cas. This is consistent with the fact that the galactic reddening in the direction of FO Per is extremely large, namely E(B-V)= 1.78, as the dust reddening in the direction of the constellation of Perseus is quite large. To estimate the reddening of FO Per, we note (Table 3) that TZ Per has a known reddening of 0.27 at a distance of about 500pc, with a galactic reddening of 0.8. Since FO Per is about half this distance but with a galactic reddening about twice as large, we assume that the reddening of FO Per is about 0.3. We carry out simulations assuming both E(B-V)=0.0 and E(B-V)=0.3, to assess the effect of the reddening on the results.

E(B-V)=0.0 For the single disk models we find little agreement between the models and the observed spectra. Assuming $M = 0.4M_{\odot}$ we find a mass accretion rate $\dot{M} = 10^{-8.5}M_{\odot}$/yr; while for the larger mass models $M = 1.2M_{\odot}$ the mass accretion rate decreases to a quiescent value $10^{-10.5}M_{\odot}$/yr. Next we try the single WD models and find that they do not provide a better fit. The lower mass models have a temperature of $\sim 25,000$K, and the higher mass models have a temperature of up to 45,000K. Because of the rather poor fit the rotational velocity does not influence the results, and we find that the 200km/s models are about as good as the 400km/s models. We then run the combined WD+disk model-fits and find the best fit to be for a $0.4M_{\odot}$ WD mass, with $T_{wd} = 21,000$K, $V_{rot} \sin i$ =200km/s, $i = 75°$, $\dot{M} = 10^{-8.5}M_{\odot}\mathrm{yr}^{-1}$, d=291pc, and the least χ^2 is 0.258. The WD contributes 29% of the FUV flux while the disk contributes 71%. This model is shown in Figure 13.

E(B-V)=0.3 The best-fit single disk model has $M_{wd} = 1M_{\odot}$, $i = 18°$, $\dot{M} = 10^{-9}M_{\odot}\mathrm{yr}^{-1}$, and gives a distance of 281pc and a much smaller χ^2, namely 0.172. The single WD model gives a smaller χ^2 but also a much smaller distance. For a $0.4M_{\odot}$ WD mass, the best fit has a temperature $T_{wd} = 35,000$K, a rotational velocity of 200km/s, and gives a distance of 135pc and $\chi^2 = 0.152$. For larger WD masses we find an even smaller distance, and we therefore disregard the single WD models. We then try the combined WD+disk models and find that a valid distance of 254pc is obtained for a $0.4M_{\odot}$ WD mass, with $T_{wd} = 40,000$K, $V_{rot} \sin i$ =200km/s, $i = 18°$, $\dot{M} = 10^{-8.5}M_{\odot}\mathrm{yr}^{-1}$, and this best model gives the least χ^2 of all 0.146. The WD contributes 52% of the FUV flux while the disk contributes the remaining 48%. This model is shown in Figure 14.

4.2.3. ES Draconis/Dra3/PG 1524+622

ES Dra has a magnitude varying between 13.9 to 16.3 (Andronov 1991; Downes et al. 2001). First suspected to be a CV by Green et al. (1986), it is classified as a SU UMa system in (Downes et al. 2001) and the non-detection of prominent superhumps indicates that it might have a low inclination (Andronov I. et al. 2003). However, its orbital period of 4.29 hr (Ringwald 1994) makes its classification as an SU UMa unlikely. ES Dra appears to sit about 1 mag below outburst for months, this is more characteristic of Z Cam systems. We therefore tentatively classify ES Dra as a Z Cam, this classification is also consistent with its location above the period gap.

ES Dra was observed with *FUSE* on 19 Nov 2006 (JD2454059). However, no AAVSO data were collected around the period of the actual *FUSE* observation. From the *FUSE* continuum flux level (2×10^{-14}ergs s^{-1}cm^{-2}Å^{-1}) it seems that ES Dra must have been in an intermediate (standstill) state possibly at 15.0-15.4 mag, where the heated WD might be the main component of the FUV continuum. The spectrum of ES Dra is shown in Figure 15.

The C III (1175) multiplet possibly exhibits a P-Cygni profile, where the broad absorption line is blue-shifted by about 3Å, and the broad emission line is red-shifted by about the same amount. This corresponds to a velocity of about $\sim$ 750km/s. Such a high velocity is probably originating close to the WD/inner disk. The C III (977) broad emission line is also red-shifted by at least 2Å. The two broad S IV absorption lines ($\sim$1063+1073) are blue shifted by 2Å, while the Si III+IV ($\sim$1110+1125) broad absorption features also show a slight blue-shift. It is clear that the C III and S IV lines are forming in an expanding shell or a corona, while the Si absorption feature also forms in the disk and atmosphere of the WD. We therefore decided to mask the C III and S IV lines in the model fitting, while keeping the Si lines.

We assume that the reddening toward ES Dra is negligible as the Galactic (maximum) reddening in that direction is itself very small: 0.03. The distance to the system inferred from the period-magnitude relation is 770pc (see Table 3), and this is the distance we use in the modeling.

Single Disk Models. The lowest χ^2 model in best agreement with a distance of 770pc is for $M = 1.2M_{\odot}$, $\dot{M} = 10^{-10}M_{\odot}$yr^{-1}, which gives a distance of 1035pc and $\chi^2 > 0.57$. The fit can be improved by changing the abundances, namely the silicon and sulfur broad absorption features are best fit when $Si \approx 10\times$ solar and $S \approx 50\times$ solar. The fit is further improved (lower χ^2) by blue-shifting the entire synthetic spectrum by 1.0Å. This best single disk model gave a distance 1754pc, and $\chi^2 = 0.4280$. This model is shown in Figure 16.

Single White Dwarf Models. We tried to fit both the distance (770pc) and the higher order of the Ly series. We first tried solar abundances models and then we increased the silicon and sulfur abundances to better fit the silicon and sulfur absorption features. The best model (Figure 17) has $T = 35,000$K, $log(g) = 7.8$ (corresponding to $M_{wd} \approx 0.58M_{\odot}$), a projected rotational velocity

$v_{rot} \sin i = 700$km/s, . Here too, we find that the best fit is obtained with $Si \approx 10\times$ solar, $S \approx 50\times$ solar and a blue-shift of 1.3Å. The distance obtained is 773pc and $\chi^2 = 0.4277$. From the point of view of the least χ^2, this model is as good as the least χ^2 single disk model, however the distance is in much better agreement with the estimate of 770pc (Table 3).

We find that WD+Disk composite models do not improve the fit, but rather the opposite.

5. Summary

We report the results of a spectroscopic analysis of a *FUSE* survey of high-declination DNs, including five Southern Hemisphere objects and three Northern Hemisphere objects. In order to model these spectra we assessed the distance and reddening of these objects and carried out a synthetic spectral fit to the observed spectra.

The low S/N in some of the spectra prevented us from obtaining robust results: for AQ Men and V433 Ara, we were only able to assess a lower limit for the WD temperature or mass accretion rate. Though we were unable to assess their distance, for HP Nor we found a WD temperature of about 40,000K and rotational velocity of 1000km/s, and for DT Aps we found a WD temperature of at least 34,000K and a rotational velocity of 500km/s.

For the 4 objects with relatively good spectra, we were able to obtain more reliable results. For NSV 10934 we find a low mass accretion rate, high inclination angle, and a large WD mass. For AM Cas the best fit model is a WD+disk composite model with a low inclination, a WD temperature T=35,000K, a mass $0.55M_{\odot}$, and a mass accretion rate of $3 \times 10^{-9} M_{\odot}$/yr. For FO Per the best fit is also a WD+ disk composite model giving $M = 0.4M_{\odot}$, T=40,000K, a low inclination and a mass accretion rate consistent with outburst ($10^{-8.5} M_{\odot}$/yr). And for ES Dra the spectrum is best fit with a single WD stellar atmosphere with T=35,000K, $M = 0.58M_{\odot}$, and a projected rotational velocity of 700km/s with over-abundant silicon and sulfur.

For 3 objects above the period gap (AM Cas, FO Per and ES Dra) we have found a WD temperature during an active state (intermediate-to-outburst) reaching 35,000-40,000K. These must be regarded as an upper limit as the WD was heated due to on-going (or recent) accretion. These temperatures are similar to the temperature of RX And on the rise to outburst (39,000K) and in decline from outburst (45,000K), while in quiescence its temperature is 34,500K (Sepinsky et al. 2002). It is therefore likely that the true temperatures of AM Cas, FO Per and ES Dra in quiescence are around 30,000-35,000K, and these objects are therefore near the average CV WD's T_{eff} above the period gap (∼30,000K), similar to U Gem, SS Aur and RX And.

We have recapitulated the effective quiescent CV WD temperatures as found in the literature in Table 5. The references are listed in the last column. Similar tables are given in the literature (Townsley & Gänsicke 2009) and sometimes reflect slightly different values, this is due to the facts that (i) for some of the systems more than one model (and therefore more than one WD

temperature) was given and we list here the best fit in which the WD contributes more than 50 percent of the flux; (ii) we also list the most recent synthetic spectral fits obtained by our own group. For WZ Sge and VW Hyi, a theoretical cooling curve of the WD was computed to fit the observed temperature decline in these systems: the quiescent temperature was the asymptotic value approached as $t \rightarrow \infty$. The temperatures listed in Table 5 are depicted in Figure 18, from which there seems to be a clear separation between Polars and DNs, both above and below the gap (Araujo-Betancor et al. 2003). VY Scl systems also seem definitely hotter than DNs. It is evident from this figure that more data points are badly needed for Z Cam systems as well as for all the CV sub-types above the gap, except maybe for U Gem's. The data points from the present work have been added as downward pointing arrows, as they are only upper limits. Since the mass and distance is not known with accuracy for many of the systems listed in Table 5, it is very likely that some of the temperatures in Table 5 will change once parallaxes and/or masses are obtained for these systems. The standard model above the gap (traditional magnetic braking Howell et al. (2001)) is between the dotted lines.

The recent work of Townsley & Gänsicke (2009) recapitulates and analyzes the effective temperatures of the WD in CVs, therefore, we wish here only to emphasize the (small) differences that we obtain above the period gap when considering the values given in Table 5. We include in the present work more data points for the VY Scl systems (BB Dor, V794 Aql, VY Scl) and DNs, and we also draw systems with $P > 5h$. Since we use the same data points for the magnetic systems, we agree that gravitational radiation can account for the WD T_{eff} (and therefore $\dot{M}$) of polars both above and below the gap. Above the gap we also agree that the majority of DNs have a temperature (mass accretion rate) lower than expected by the standard theory, and that NL VY systems have a temperature higher than expected from the standard theory. However, we find that the traditional magnetic braking could explain the temperature (mass accretion rate) of some systems (TU Men, BB Dor, SS Aur, U Gem) above the period gap.

Overall it seems that the standard model (and any modified model: see Townsley & Gänsicke (2009) for a discussion) does not agree with the non-magnetic CVs above the period gap. While it is difficult to explain the discrepancy above the gap between the theory and observations for the DN systems, a higher than expected temperature for the NL VY can be accounted for with a higher mass accretion rate $< \dot{M} >$.

PG wishes to thank Mario Livio, for his kind hospitality at the Space Telescope Science Institute where part of this work was carried out. We wish to thank the members of the American Association of Variable Star Observers (AAVSO), the Austral Variable Star Observer Network (AVSON), and the Center for Backyard Astrophysics (CBA) for providing us with optical monitoring of Northern and Southern hemisphere systems, as well as optical archival data on these systems. This research was based on observations made with the NASA-CNES-CSA Far Ultraviolet Spectroscopic Explorer. *FUSE* is operated for NASA by the Johns Hopkins University under NASA contract NAS5-32985. This work was supported by the National Aeronautic and Space Admin-

istration (NASA) under FUSE Cycle 7 (Guest Investigator Program) grant NNX06AD28G and supported in part by NSF grant AST0807892, both to Villanova University. This publication also makes use of the data products from the Two Micron All Sky Survey, which is a joint project of the University of Massachusetts and the Infrared Processing and Analysis Center/California Institute of Technology, funded by the National Aeronautics and Space Administration and the National Science Foundation.

REFERENCES

Andronov, I.L. 1991, Commission 27 of the IAU, Information Bulletin on Variable Stars, p.3645

Andronov, I.L. et al. 2003, ASP Conference Series, Vol. 292, *Interplay of Periodic, Cyclic and Stochastic Variability in Selected Areas of the H-R Diagram*, ed. C. Sterken, p.313

Andronov, N., Pinsonneault, & Sills, A. 2003, ApJ, 582, 358

Araujo-Betancor, S., et al. 2003, ApJ, 583, 437

Araujo-Betancor, S., Gänsicke, B.T., Long, K.S., Beuermann, K., de Martino, D., Sion, E.M., & Szkody, P. 2005, ApJ, 622, 589

Basri, G. 1987, ApJ, 316, 377

Beuermann, K., Wheatley, P., Ramsay, G., Euchner, F., & Gänsicke, B.T. 2000, A&A, 354, L49

Bruch, A., & Engel, A. 1994, A&AS, 104, 79

Bruch, A., et al. 1987, A&A, 70, 481

Bruch, A. 1989, A&AS, 78, 145

Cheng, A., O'Donoghue, D., Stobie, R.S., Kilkenny, D., & Warner, B. 2001, MNRAS, 325, 89

Clemens, C.J., Reid, N.I., Gizis, J.E., & O'brian, S.M. 1998, ApJ, 496, 352

Dixon, W.V., et al. 2007, PASP, 119, 527

Downes, R.A., Webbink, R.F., Shara, M.M., Ritter, H., Kolb, U., & Duerbeck, H.W. 2001, PASP, 113, 764

Eggleton, P.P. 1976, IAU Symp. 73, 209

Faulkner, J. 1971, ApJ, 170, L99

Gänsicke, B.T. 1999, in ASP Conf. Ser. 157, Annapolis Workshop on Magnetic Cataclysmic Variables, ed. C. Hellier & K. Mukai (San Francisco: ASP), 261

Gänsicke, B.T. 2005, ASPC, 330, 3

Gänsicke, B.T, & Koester, D. 1999, A&A, 346, 151

Gänsicke, B.T., Beuermann, K., de Martino, D., & Thomas, H.-C. 2000, A&A, 354, 605

Gänsicke, B.T, Long, K.S., Barstow, M.A., & Hubney, I. 2006, ApJ, 639, 1039

Gänsicke, B.T, Sion, E.M., Beuermann, K., Fabian, D., Cheng, F.H., & Krautter, J. 1999, A&A, 347, 178

Gänsicke, B.T., et al. 2003, ApJ, 594, 443

Gänsicke, B.T., Szkody, P., Howell, S.B., & Sion, E.M. 2004, ApJ, 629, 451

Gessner, H. 1978, Mitt. Veränderl. Sterne, 8, 66

Godon, P., 2007, unpublished

Godon, P., & Sion, E.M. 2005, MNRAS, 361, 809

Godon, P., Seward, L., Sion, E.M., & Szkody, P. 2006a, AJ, 131, 2634

Godon, P., Sion, E.M., Cheng, F., Long, K.S., Gänsicke, B.T., & Szkody, P. 2006b, ApJ, 642, 1018

Godon, P., Sion, E.M., Barrett, P., & Szkody, P. 2007, ApJ, 656, 1092

Godon, P., Sion, E.M., Barrett, P.E., Hubeny, I., Linnell, A.P., & Szkody, P. 2008a, ApJ, 679, 1447

Godon, P., Sion, E.M., Barrett, P.E., Szkody, P., & Schlegel, E.M. 2008b, ApJ, 687, 532

Green, R.F., Schmidt, M., & Liebert, J. 1986, ApJS, 61, 305

Hack, M., & La Dous, C. 1993, *Cataclysmic Variables and Related Objects*, (NASA SP-507)/US Gov. Printing Office

Hamada, T., & Salpeter, E.E. 1961, ApJ, 134, 683

Hameury, J.M., King, A.R., Lasota, J.P., Ritter, H. 1988, MNRAS, 231, 535

Hameury, J.M., King, A.R., Lasota, J.P. 1990, MNRAS, 242, 141

Hamilton, R.T., & Sion, E.M. 2004, PASP, 116, 926

Hamilton, R.T., & Sion, E.M. 2008, PASP, 120, 165

Harrison, T.E., Johnson, J.J., McArthur, B.E., Benedict, G.F., Szkody, P., Howell, S.B., & Gelino, D.M. 2004, AJ, 127 460

Hartely, L.E., Long, K.S., Froning, C.S., & Drew, J.E. 2005, ApJ, 623, 425

Hoard, D.W., Linnell, A.P., Szkody, P., Fried, R.E., Sion, E.M., Hubeny, I., & Wolfe, M.A. 2004, ApJ, 604, 346

Hoffmeister, C. 1929, Astron.Nach., 234, 33

Howarth, I.D. 1976, Mitt. Veränderl. Sterne, 7, 147

Howell, S.B., Gänsicke, B.T., Szkody, P., & Sion, E.M. 2002, ApJ, 575, 419

Howell, S.B., Nelson, L.A., & Rappaport, S. 2001, ApJ, 550, 897

Hubeny, I. 1988, Comput. Phys. Commun., 52, 103

Hubeny, I.,& Lanz, T. 1995, ApJ, 439, 875

Ivanova, N., & Taam, R.E. 2004, ApJ, 601, 1058

Kato, R. et al. 2002, A&A, 396, 929

Kato, R. et al. 2004, MNRAS, 347, 861

King, A.R. 1988, QJRAS, 29, 1

King, A.R., Schenker, K., & Hameury, J.M. 2002, MNRAS, 335, 513

Knigge, C. 2006, MNRAS, 373, 484

Knigge, C. 2007, MNRAS, 382, 1982

Kolb, U. 1993, A&A, 271, 149

Kolb, U., & Baraffe, I. 1999, MNRAS, 309, 1034

Kolb, U., Rappaport, S., Schenker, K., & Howell, S.B. 2001, ApJ, 563, 958

Long, K.S., & Gilliland, R.L. 1999, ApJ, 511, 916

McCormick, P., & Frank, J. 1998, ApJ, 500, 923

Mc Dermott, P.N., & Taam, R.E. 1989, ApJ, 342, 1019

Munari, U., & Zwitter, T. 1998, A&AS, 128, 277

Notni, P., & Richter, G.A. 1984, Inf.Bull. Variable Stars No. 2634

Paczyński, B., & Sienkiewicz, R. 1981, ApJ, 248, L27

Paczyński, B., & Sienkiewicz, R. 1983, ApJ, 268, 825

Pandel, D., Córdova, F.A., & Howell, S.B. 2003, MNRAS, 346, 1231

Pandel, D., Córdova, F.A., Mason, K.)., & Priedhorsky, W.C. 2005, ApJ, 626, 396

Panei, J.A., Althaus, L.G., & Benvenuto, O.G. 2000, A&A, 353, 970

Patterson, J., 1984, ApJS, 54, 443

Patterson, J. 2002, http://cbastro.org/communications/news/2002/march28.html

Press, W.H., Teukolsky, S.A., Vetterling, W.T., Flannery, B.P., Numerical Recipes in Fortran 77, The Art of Scientific Computing, Second Edition, 1992, Cambridge University Press.

Pretorius, M.L., Warner, B., & Woudt, P.A. 2006, MNRAS, 368, 361

Price, A., 2006, AAN, 339, 1

Puebla, R.E., Diaz, M.P., Hubeny, I. 2007, 134, 1923

Rappaport, S., Joss, P.C., & Webbink, R.F. 1982, ApJ, 254, 616

Rappaport, S., Verbunt, F., & Joss, P.C. 1983, ApJ, 275, 713

Richter, G.A. 1961, Veröff.Sternw.Sonneberg, 4, 433

Richter, G.A., Notni, P., & Tiersch, H. 1988, Astron.Nach., 309, 91

Ringwald, R.A. 1994, *Interacting Binary Stars*, ASP Conferences Series, Vol. 56, A.W. Shafter (ed.), p.294

Ritter H., & Kolb U. 2003, A&A, 404, 301 <http://physics.open.ac.uk/RKcat/RKcat_AA.ps>

Robinson, E.L. 1976, ARA&A, 14, 119

Rosen, S.R., et al. 2001, MNRAS, 322, 631

Schenker, K., Kolb, U., & Ritter, H. 1998, MNRAS, 297, 633

Schlegel, D.J., Finkbeiner, D.P., & Davis, M. 1998, ApJ, 500, 525

Sepinsky, J.F., Sion, E.M., Szkody, P., & Gänsicke, B.T. 2002, ApJ, 574, 937

Shakura, N.I., & Sunyaev, R.A., 1973, A&A, 24, 337

Sheets, H.A., Thorstensen, J.R., Peters, C.J., Kapusta, A.B., & Taylor, C.J., 2007, PASP, 119, 494

Schwope, A.D., Hambarayan, V., Schwarz, R., Kanbach, G., & Gänsicke, B.T. 2002, A&A, 392, 541

Sion, E.M., 1991, AJ, 102, 295

Sion, E.M., & Godon, P. 2009, in preparation

Sion, E.M., Cheng, F.H., Szkody, P., Sparks, W., Gänsicke, B.T., Huang, M., & Mattei, J. 1998, ApJ, 496, 449

Sion, E.M., Gänsicke, B.T., Long, K.S., Szkody, P., Knigge, C., Hubeny, I., de Martino, D., & Godon, P. 2008, ApJ, 681, 543

Sion, E.M., Godon, P., Cheng, F., & Szkody, P. 2007, AJ, 134, 886

Sion, E.M., Szkody, P., Cheng, F., Gänsicke, B.T., & Howell, S.B. 2003, ApJ, 583, 907

Sion, E.M., Szkody, P., Gänsicke, B.T., Cheng, F.H., LaDous, C., & Hassall, B. 2001, ApJ, 555, 834

Spruit, H.C., & Ritter, H. 1983, A&A, 124, 267

Spruit, H.C., & Taam, R.E. 2001, ApJ, 548, 900

Szkody, P., Gänsicke, B.T., Sion, E.M., Howell, S.B., & Cheng, F.H. 2003, A&A, 126, 1451

Szkody, P., Gänsicke, B.T., Howell, S.B., & Sion, E.M. 2002, ApJ, 575, L79

Szkody, P., Sion, E.M., Gänsicke, B.T., & Howell, S.B., 2002, in ASP Conf.Ser. 261, The Physcis of Cataclysmic Variables and Related Objects, ed. B.T. Gänsicke, K. Beuermann, & K. Reinsch (San Francisco: ASP), 21

Taam, R.E., Sandquist, E.L., & Dubus, G. 2003, ApJ, 592, 1124

Taam, R.E., & Spruit, H.C. 2001, ApJ, 561, 329

Townsley, D., & Bildsten, L. 2003, ApJ, 596, L227

Townsley, D., & Bildsten, L. 2004, ApJ, 600, 390

Townsley, D., & Gänsicke, B.T. 2009, ApJ, 693, 1007

Taylor, C.J., & Thorstensen, J.R. 1996, PASP, 108, 894

Urban, J.A., & Sion, E.M. 2006, ApJ, 642, 1029

Verbunt, F. & Zwaan, C. 1981, A&A, 100, L7

Vogt, N., & Bateson, F.M. 1982, A&AS, 48, 383

Wade, R.A., & Hubeny, I. 1998, ApJ, 509, 350

Warner, B. 1987, MNRAS, 227, 23

Warner, B. 1995, Cataclysmic Variable Stars (Cambridge: Cambridge Univ. Press)

Weber, E.J. & Davis, L. 1967, ApJ, 148, 217

Webbink, R.F. 1981, BAAS, 12, 848

Whyte, C.A., & Eggleton, P.P. 1980, MNRAS, 190, 801

Wood, M.A. 1995, in White Dwarfs, Proceedings of the 9th European Workshop on White Dwarfs, Lecture Notes in Physics, Vol.442, eds. Detlev Koester & Klaus Werner, Springer-Verlag, Berlin Heidelberg New York, p.41

Woudt, P.A., Warner, B., & Spark, M. 2005, MNRAS, 364, 107

Table 1. System Parameters of the *FUSE* Targets

Name[a]	Type	P_{orb} (hr)	i (deg)	V_{max}	V_{min}	Priority
VW Tuc	UG	—	> 20?	15.2	< 16.5	2
AQ Men	UG/NL?	3.40	eclipsing	14	15	1
HP Nor	ZC	—	—	12.8	16.4	2
IK Nor	UG	—	—	12.9	16.3	2
V663 Ara	SU	—	—	15.9	< 16.3	2
V433 Ara	ZC/NL?	4.70	—	14.8	< 16.3	2
V499 Ara	UG	—	—	14.8	< 16.2	2
DT Aps	SS	—	—	14.4	< 15.8	1
NSV 10934	SU	1.74	—	11.2	15.0	1
AM Cas	ZC	3.96	—	12.3	15.2	1
FO Per	UG	3.52/4.13	—	11.8	16.2	1
ES Dra	ZC	4.29	low?	13.9	16.3	1

[a]The Targets are listed in order of ascending RA, Southern Hemisphere objects followed by Norther Hemisphere objects.

Table 2. FUSE Observations Log

System Name	Date (dd/mm/yy)	Exp.time (sec)	Dataset	Aperture	Operation Mode	V	State	Data Quality
VW Tuc	11-06-06	8,835	G9250101	LWRS	TTAG	16-18?	quiescence	unusable
AQ Men	22-11-06	22,661	G9250201	LWRS	TTAG	14-15	usual state	poor
HP Nor	13-04-07	3,952	G9250601	LWRS	TTAG	15.0	low	poor
IK Nor	13-04-07	7,947	G9250701	LWRS	TTAG	—	—	unusable
V663 Ara	12-04-07	4,807	G9250802	LWRS	TTAG	—	—	unusable
	24-04-06	9,785	G9250801	LWRS	TTAG	—	—	unusable
V433 Ara	18-02-07	7,009	G9250901	LWRS	TTAG	—	—	unusable
V499 Ara	22-06-06	17,988	G9251001	LWRS	TTAG	—	—	unusable
DT Aps	03-05-06	8,053	G9251102	LWRS	TTAG	—	decline/low	unusable
	28-04-06	68,245	G9251101	LWRS	TTAG	—	active	poor
NSV 10934	28-06-06	11,956	G9251201	LWRS	TTAG	—	—	poor
	30-06-06	14,177	G9251202	LWRS	TTAG	—	—	poor
AM Cas	19-10-06	12,909	G9251402	LWRS	TTAG	13.3-13.8	intermediate	good
FO Per	11-02-07	2,716	G9251501	LWRS	TTAG	13.5	intermediate	good
ES Dra	19-11-06	24,554	G9251601	LWRS	TTAG	15.1-15.4	intermediate	good

Table 3. Parameters Adopted for the Modeling

System Name	Period (hr)	Gal.Lat. (deg)	E^{Gal}_{B-V}	E^{adp}_{B-V}	d_w (pc)	d_h (pc)	d_k (pc)	d (pc)
HP Nor	—	-3	0.63	0.20	—	—	—	—
DT Aps	—	-20	0.09	0.09	—	—	—	—
NSV 10934	1.74	-27	0.16	0.10	151	155	117-219	150
AQ Men	3.40	-31	0.18	0.10	664	752	201-377	710
FO Per	3.52	0	1.78	0.30	244	279	182-342	260
	4.13	0	1.78	0.30	262	311	227-311	285
AM Cas	3.96	9	0.89	0.20	324	380	153-287	350
ES Dra	4.29	47	0.02	0.00	702	840	540-1016	770
V433 Ara	4.70	-9	0.19	0.10	1114	1368	747-1411	1200
TZ Per	6.31	-3	0.78	0.27	424	575	—	500

[–]The systems are listed in order of increasing binary period. In column (3) we list the Galactic Latitude. In column (4) we list the Galactic reddening which is anti-correlated to the Galactic Latitude. as inferred from the 100μm dust emission map (Schlegel et al. 1998). In column (5) we list the reddening we used in our modeling. In column (6) we list the distance assessed using the period-magnitude correlation given by Warner (1987). In column (7) we list the distance assessed using the period-magnitude correlation given by Harrison et al. (2004). In column (8) we list the distance estimated using the secondary IR emission technique of Knigge (2006, 2007). In the last column we list the distance we used in our modeling. TZ Per was not observed but has been added for comparison.

Table 4. Synthetic Spectra

System Name	M_{wd} ($M_\odot$)	T_{wd} (10^3K)	$V_{rot}sini$ (km/s)	i (deg)	$Log(\dot{M})$ ($M_\odot$/yr)	WD/Disk (%)	d (pc)	χ^2_ν	E_{B-V}	Fig.
HP Nor	0.4	34	1000	—	—	WD	1134	0.105	0.00	
	0.8	37	1000	—	—	WD	648	0.107	0.00	
	1.2	40	1000	—	—	WD	381	0.105	0.00	
	0.55	—	—	60	-8.5	Disk	1448	0.105	0.00	
	0.8	—	—	< 41	-9.0	Disk	1603	0.104	0.00	
	1.2	—	—	8	-10.0	Disk	1021	0.101	0.00	
	0.4	40	1000	—	—	WD	530	0.096	0.20	
	0.8	43	1000	—	—	WD	265	0.096	0.20	3
	1.2	46	1000	—	—	WD	148	0.096	0.20	
	0.55	—	—	18	-8.0	Disk	1060	0.097	0.20	
	0.8	—	—	18	-8.0	Disk	1800	0.093	0.20	
	1.2	—	—	18	-8.5	Disk	1515	0.095	0.20	
AQ Men	0.4	24	—	—	—	WD	710	—	0.00	
	1.1	36	—	—	—	WD	710	—	0.00	
	0.35	—	—	81	-8.75	Disk	710	—	0.00	
	1.20	—	—	81	-9.5	Disk	710	—	0.00	
	0.4	28.5	—	—	—	WD	710	—	0.10	
	1.1	60	—	—	—	WD	710	—	0.10	
	0.35	—	—	81	-7.9	Disk	710	—	0.10	
	1.20	—	—	81	-8.9	Disk	710	—	0.10	
V433 Ara	0.4	—	—	81	-8.5	Disk	1200	—	0.00	
	0.4	—	—	81	-8.0	Disk	1200	—	0.10	
	1.2	—	—	81	-9.5	Disk	1200	—	0.00	
	1.2	—	—	81	-9.0	Disk	1200	—	0.10	
	0.4	24	—	—	—	WD	1200	—	0.00	
	0.4	28	—	—	—	WD	1200	—	0.10	
	0.8	30	—	—	—	WD	1200	—	0.00	
	0.8	40	—	—	—	WD	1200	—	0.10	
	1.2	40	—	—	—	WD	1200	—	0.00	
	1.2	75	—	—	—	WD	1200	—	0.10	
DT Aps	≤ 1.2	—	—	18	≥ -10	Disk	≥ 2800	0.213	0.00	

Table 4—Continued

System Name	M_{wd} ($M_\odot$)	T_{wd} (10^3K)	$V_{rot}sini$ (km/s)	i (deg)	$Log(\dot{M})$ ($M_\odot$/yr)	WD/Disk (%)	d (pc)	χ^2_ν	E_{B-V}	Fig.
	≤ 1.2	—	—	18	≥ -9.5	Disk	≥ 2950	0.223	0.09	
	≥ 0.4	≥ 34	500	—	—	WD	≥ 1000	0.212	0.00	
	0.8	37	500	—	—	WD	1700	0.205	0.00	8
	≥ 0.4	≥ 36	500	—	—	WD	≥ 625	0.225	0.09	
NSV 10934	0.8	—	—	75	-10	Disk	185	0.196	0.00	
	1.2	—	—	81	-10.5	Disk	144	0.160	0.00	
	0.4	—	—	75	-9	Disk	179	0.202	0.10	
	0.8	—	—	80	-9.5	Disk	157	0.172	0.10	
	1.2	—	—	81	-10	Disk	187	0.146	0.10	11
	1.2	30	—	—	—	WD	216	0.232	0.10	
AM Cas	≤ 0.8	—	—	≤ 60	≥ -9.5	Disk	350	0.611	0.00	
	0.40	30	1000	—	—	WD	307	0.623	0.00	
	0.80	36	500	18	-9.7	41/59	373	0.563	0.00	14
	0.55	35	400	18	-8.5	11/89	331	0.538	0.20	15
FO Per	0.40	—	—	75	-8.5	Disk	251	0.296	0.00	
	0.80	—	—	60	-9.5	Disk	295	0.313	0.00	
	$\geq$0.40	$\geq$25	400	—	—	WD	266	$\geq$0.312	0.00	
	0.40	21	200	75	-8.5	29/71	291	0.258	0.00	18
	1.00	—	—	18	-9.0	Disk	281	0.172	0.30	
	≥ 0.40	35	200	—	—	WD	$\leq$135	0.152	0.30	
	$\geq$0.40	40	200	18	$\leq$-8.5	52/48	$\leq$254	0.146	0.30	19
ES Dra	1.20	—	—	5	-9.5	Disk	770	0.4280	0.00	22
	0.58	35	700	—	—	WD	770	0.4277	0.00	23

Table 5. CV WD Temperatures in Quiescence

Name[a]	Type	P_{orb} (min)	T_{wd} (K)	Reference
GW Lib	DN SU	76.8	13,300	Szkody et al. (2002a)
BW Scl	DN SU	78.2	14,800	Gänsicke et al. (2004)
LL And	DN SU	79.2	14,300	Howell et al. (2002)
EF Eri	NL AM	81.0	9,500	Beuermann et al. (2000)
WZ Sge	DN SU	81.6	13,500	Godon et al. (2006b)
AL Com	DN SU	81.6	16,300	Szkody et al. (2003)
SW UMa	DN SU	81.8	14,000	Gänsicke et al. (2004); Urban & Sion (2006)
HV Vir	DN SU	83.5	13,300	Szkody et al. (2002b)
WX Cet	DN SU	83.9	14,500	Sion et al. (2003); Urban & Sion (2006)
T Leo	DN SU	84.7	16,000	Hamilton & Sion (2004)
EG Cnc	DN SU	86.4	13,300	Szkody et al. (2002b)
DP Leo	NL AM	89.8	13,500	Schwope et al. (2002)
V347 Pav	NL AM	90.0	12,300	Araujo-Betancor et al. (2005)
BC UMa	DN SU	90.2	15,200	Gänsicke et al. (2004); Urban & Sion (2006)
VY Aqr	DN SU	90.8	14,000	Sion et al. (2003); Urban & Sion (2006)
EK TrA	DN SU	91.6	17,000	Godon et al. (2008a)
BZ UMa	DN SU	97.9	17,500	Godon (2008); Urban & Sion (2006)
VV Pup	NL AM	100.4	12,100	Araujo-Betancor et al. (2005)
V834 Cen	NL AM	101.5	14,200	Araujo-Betancor et al. (2005)
HT Cas	DN SU	106.1	18,000	Urban & Sion (2006)
VW Hyi	DN SU	106.9	19,000	Sion & Godon (2009)
CU Vel	DN SU	113.0	18,500	Gänsicke & Koester (1999)
BL Hyi	NL AM	113.6	13,100	Araujo-Betancor et al. (2005)
MR Ser	NL AM	113.5	14,000	Araujo-Betancor et al. (2005)
ST LMi	NL AM	113.9	10,800	Araujo-Betancor et al. (2005)
EF Peg	DN SU	123.0	16,600	Howell et al. (2002)
HU Aqr	NL AM	125.0	14,000	Gänsicke (1999)
UV Per	DN SU	125.0	20,000	Urban & Sion (2006)
QS Tel	NL AM	139.9	17,500	Rosen et al. (2001)
TU Men	DN UG	168.8	28,000	Sion et al. (2008)
AM Her	NL AM	185,6	19,800	Gänsicke et al. (2006)
MV Lyr	NL VY	191.0	47,000	Hoard et al. (2004)

Table 5—Continued

Name[a]	Type	P_{orb} (min)	T_{wd} (K)	Reference
DW UMa	NL SW	196.7	50,000	Araujo-Betancor et al. (2003)
TT Ari	NL VY	198.0	39,000	Gänsicke et al. (1999)
BB Dor	NL VY	214.8	32,000	Godon et al. (2008b)
V794 Aql	NL VY	220.8	47,000	Godon et al. (2007)
UU Aql	DN UG	235.5	27,000	Sion et al. (2007)
X Leo	DN UG	237.0	33,000	Urban & Sion (2006)
AM Cas	DN ZC	237.6	<35,000	this work
VY Scl	NL VY	239.3	45,000	Hamilton & Sion (2008)
FO Per	DN UG	229.5[a]	<40,000	this work
V1043 Cen	NL AM	251.4	15,000	Gänsicke et al. (2000)
WW Cet	DN	253.1	26,000	Godon et al. (2006a)
U Gem	DN UG	254.7	31,000	Sion et al. (1998); Long & Gilliland (1999); Urban & Sion (2006)
ES Dra	DN ZC	257.4	<35,000	this work
SS Aur	DN UG	263.2	34,000	Godon et al. (2008a)
V895 Cen	NL AM	285.9	13,800	Araujo-Betancor et al. (2005)
RX And	DN ZC	302.2	34,000	Sion et al. (2001); Urban & Sion (2006)
TT Crt	DN UG	386.4	30,000	Sion et al. (2008); Urban & Sion (2006)
SS Cyg	DN UG	396.2	55,000	Sion et al. (2007)
Z Cam	DN ZC	417.4	57,000	Hartley et al. (2005)
RU Peg	DN UG	539.4	70,000	Godon et al. (2008a)
EY Cyg	DN UG	661.4	30,000	Godon et al. (2008a)
V422 Cen	DN UG	662.4	47,000	Sion et al. (2008)
BV Cen	DN UG	878.6	40,000	Sion et al. (2007)

[a]For FO Per it is not known whether the period is 211.2min or 247.8min, we therefore took the intermediate value 229.5min for practical reasons.

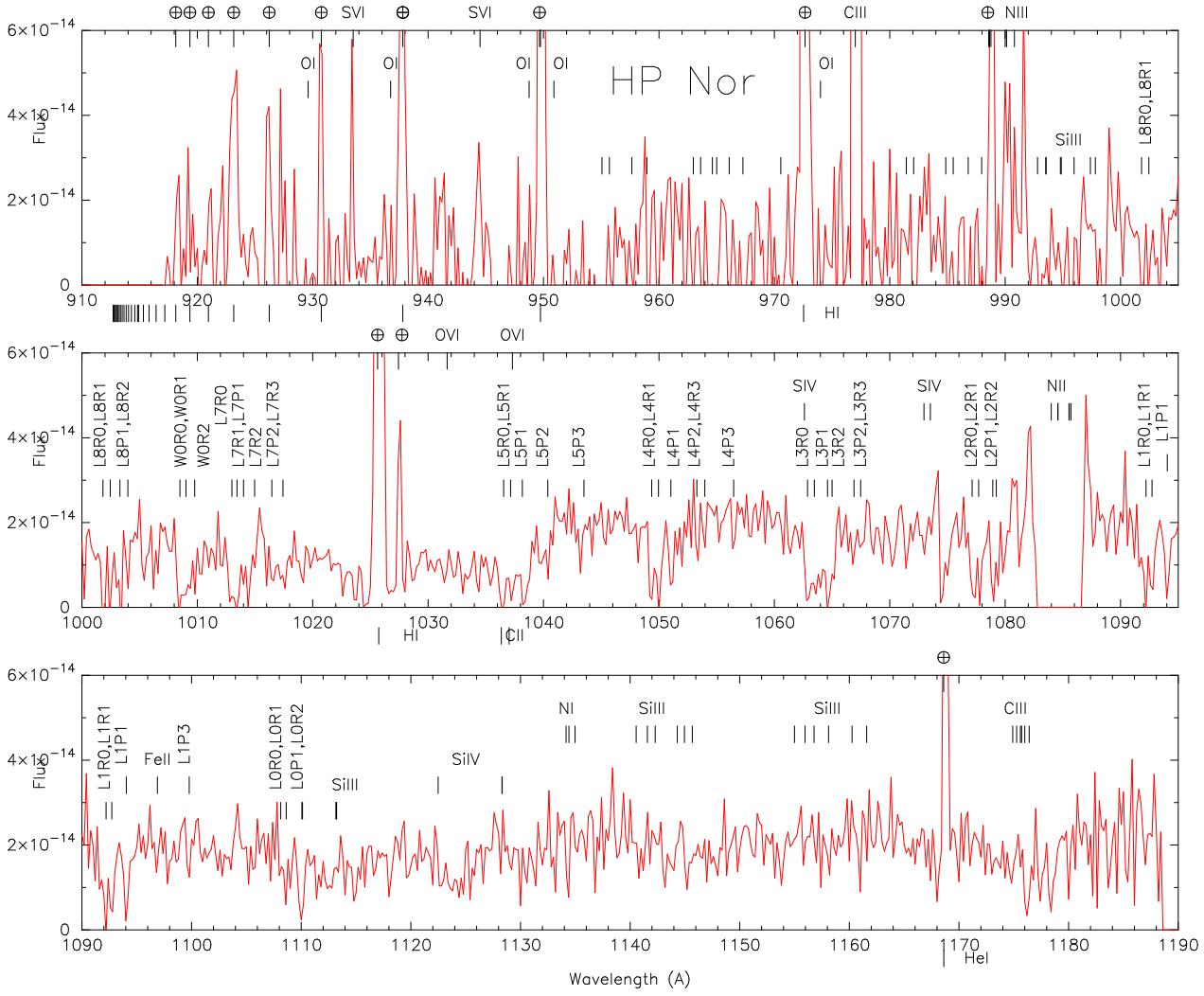

Fig. 1.— The *FUSE* spectrum of HP Nor. The sharp emission lines (including S VI 944 Å) are due to geo- and helio-coronal contamination. The ISM molecular features are denoted for clarity. The C III (1175Å) absorption feature is identified possibly with a red shift of $\sim$ 2Å. The S IV (1073Å), Si III (1113Å), Si IV (1122 & 1128Å) lines could also be accounted for with a red-shift of $\sim$ 2Å. Other metal lines have been marked but are not detected.

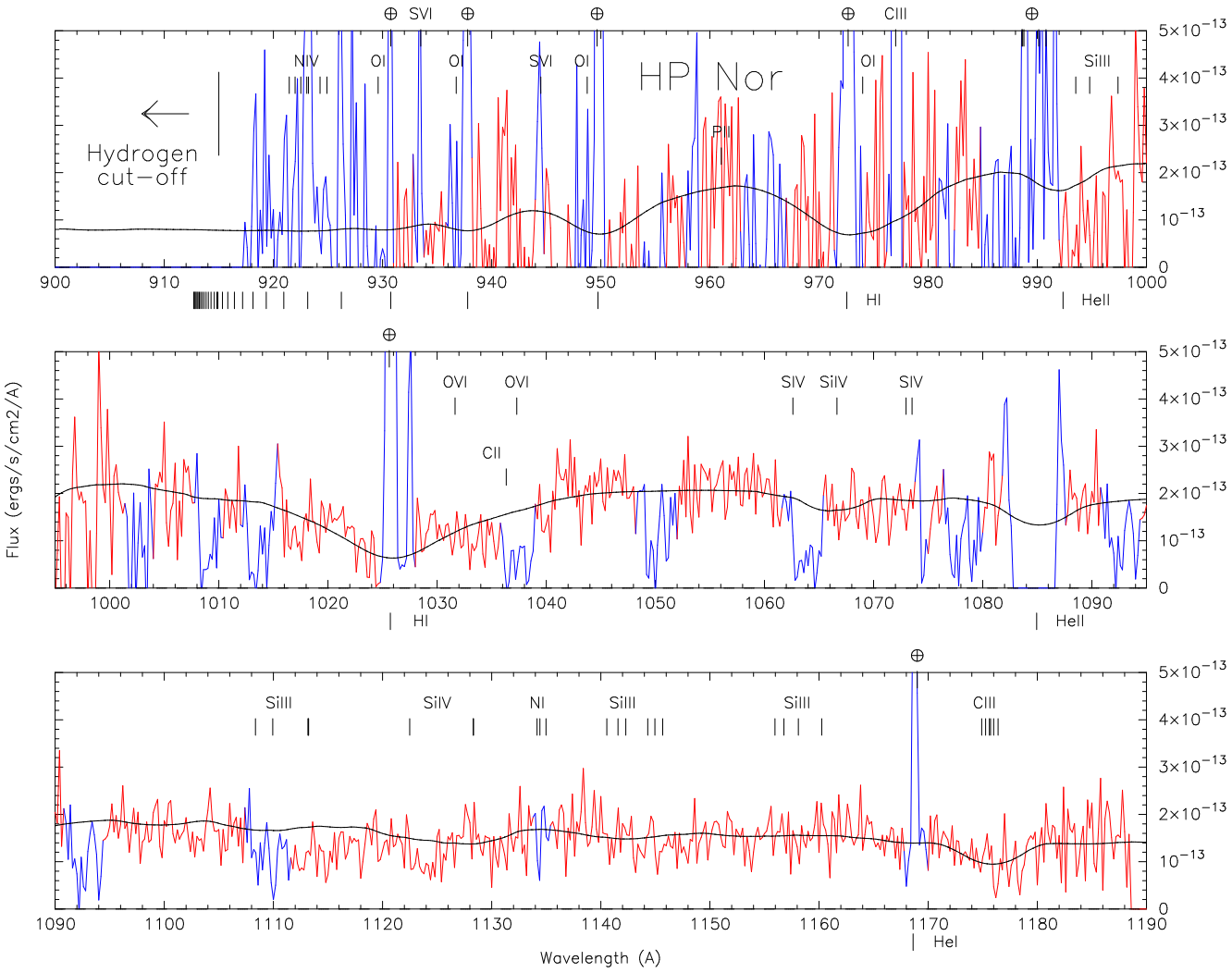

Fig. 2.— The best fit model to the *FUSE* spectrum of HP Nor assuming E(B-V)=0.2. The model is in black, the observed spectrum in red (light gray), and the regions that have been masked before the fitting are in blue (dark gray). The model consists of a WD with $M = 0.8 M_{\odot}$, T=43,000K, and a projected rotational velocity $v_{rot} \sin i = 1000$km/s. The distance obtained is d=265pc.

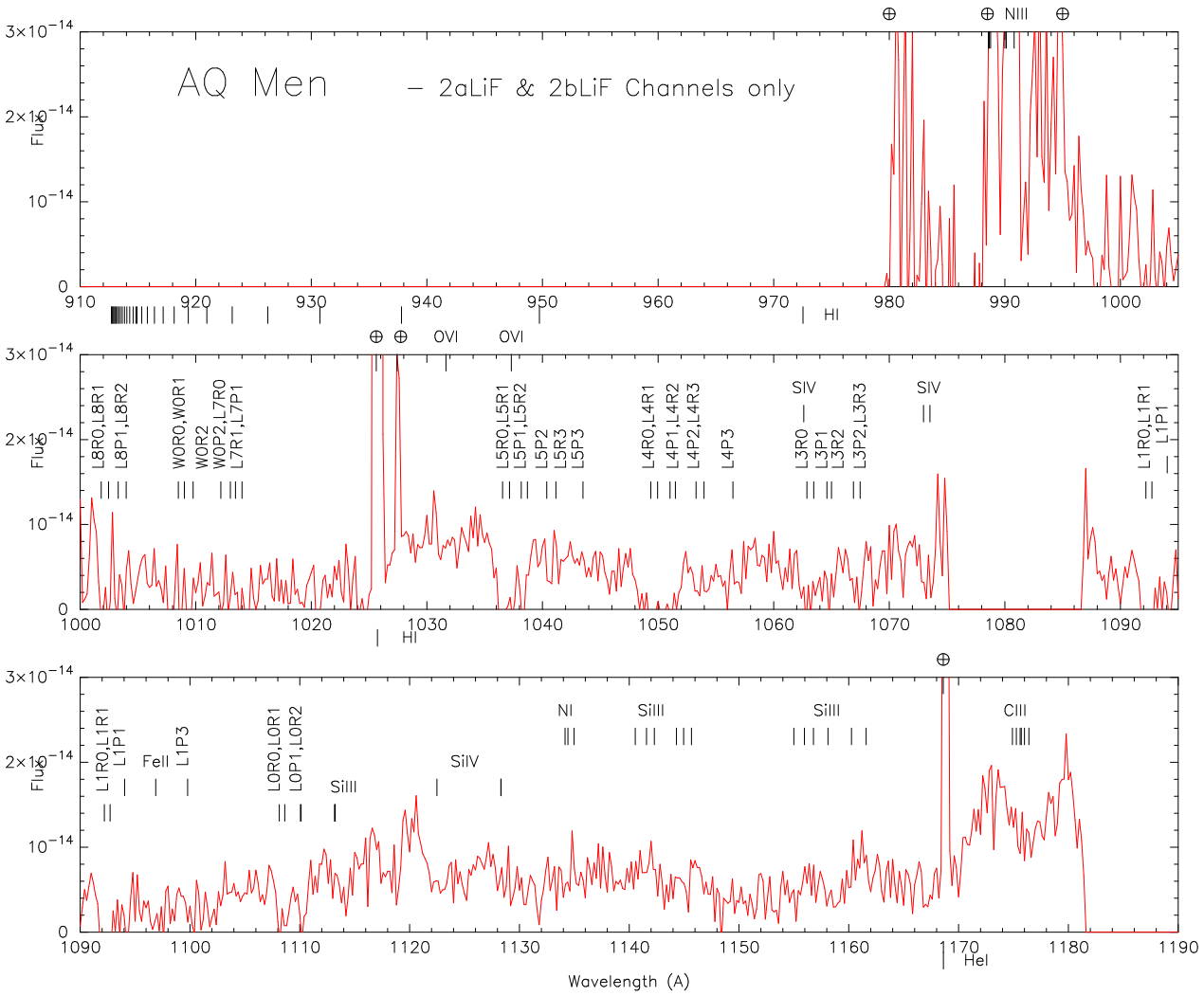

Fig. 3.— The *FUSE* spectrum of AQ Men. Due to their contamination with air glow and very low signal, the LiF 1 and SiC 1 & 2 channels have been discarded. Even though the signal is very poor, one recognizes the ISM molecular absorption features (labelled vertically), as well as some broad emission from C III (1175) and the O VI doublet. One can identify the Si III (1113Å) and Si IV (1123 & 1128Å) lines. Other metal lines have been marked but are not detected.

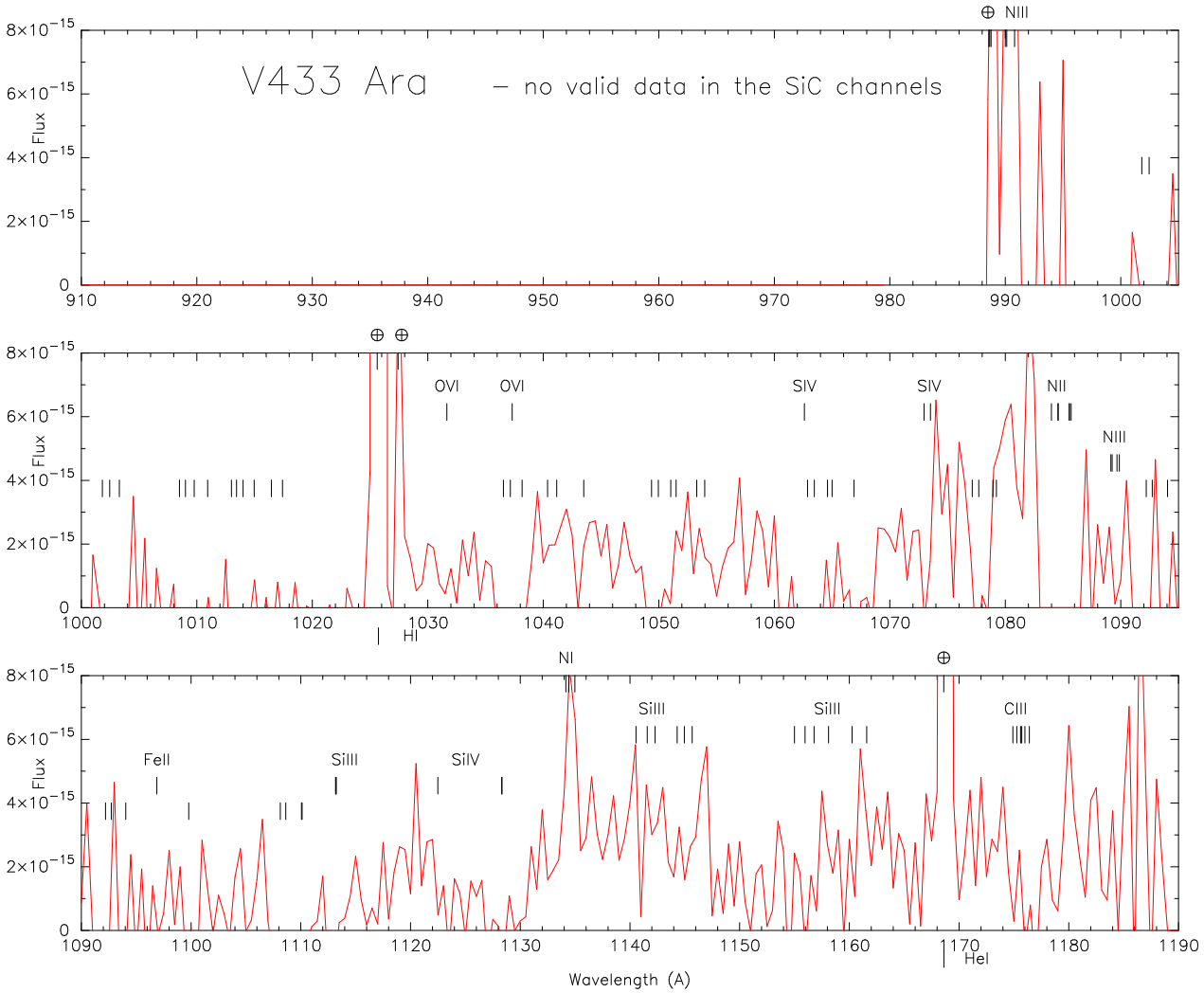

Fig. 4.— The *FUSE* spectrum of V433 Ara. Due to their contamination with air glow and very low signal, the SiC 1 & 2 channels have been discarded. The S/N is so poor that it is impossible to model any features, instead the flux level is used to assess a limit on the WD temperature and/or the disk mass accretion rate. We have marked the ISM molecular lines as well as the metals lines usually seen in spectra of quiescent DNs. Some lines coincide (e.g. C III 1175Å) with a dip in the flux, but no lines are actually detected as the flux also dips in region where lines are not expected to be observed (e.g. 1150Å).

Fig. 5.— The *FUSE* spectrum of DT Aps. In the upper panel the spectrum consists mainly of sharp air glow emission lines; at longer wavelengths, in the middle panel, the spectrum reveals a prominent broad and deep Lyβ absorption feature. In the longer wavelengths (lower panel) the silicon absorption features Si III & Si IV (around $\lambda \sim 1110 - 1130$Å) are very deep and there seems to be some emission around $\lambda \sim 1150 - 1160$Å , both could be due to an incorrect background subtraction. The broad C III (λ1175) absorption feature is the sign of a large velocity broadening. The only lines that are identified are the ISM molecular lines and the C III (1175Å) line, all the other lines have been marked but are not detected. Overall the spectrum is rather noisy and of a poor quality.

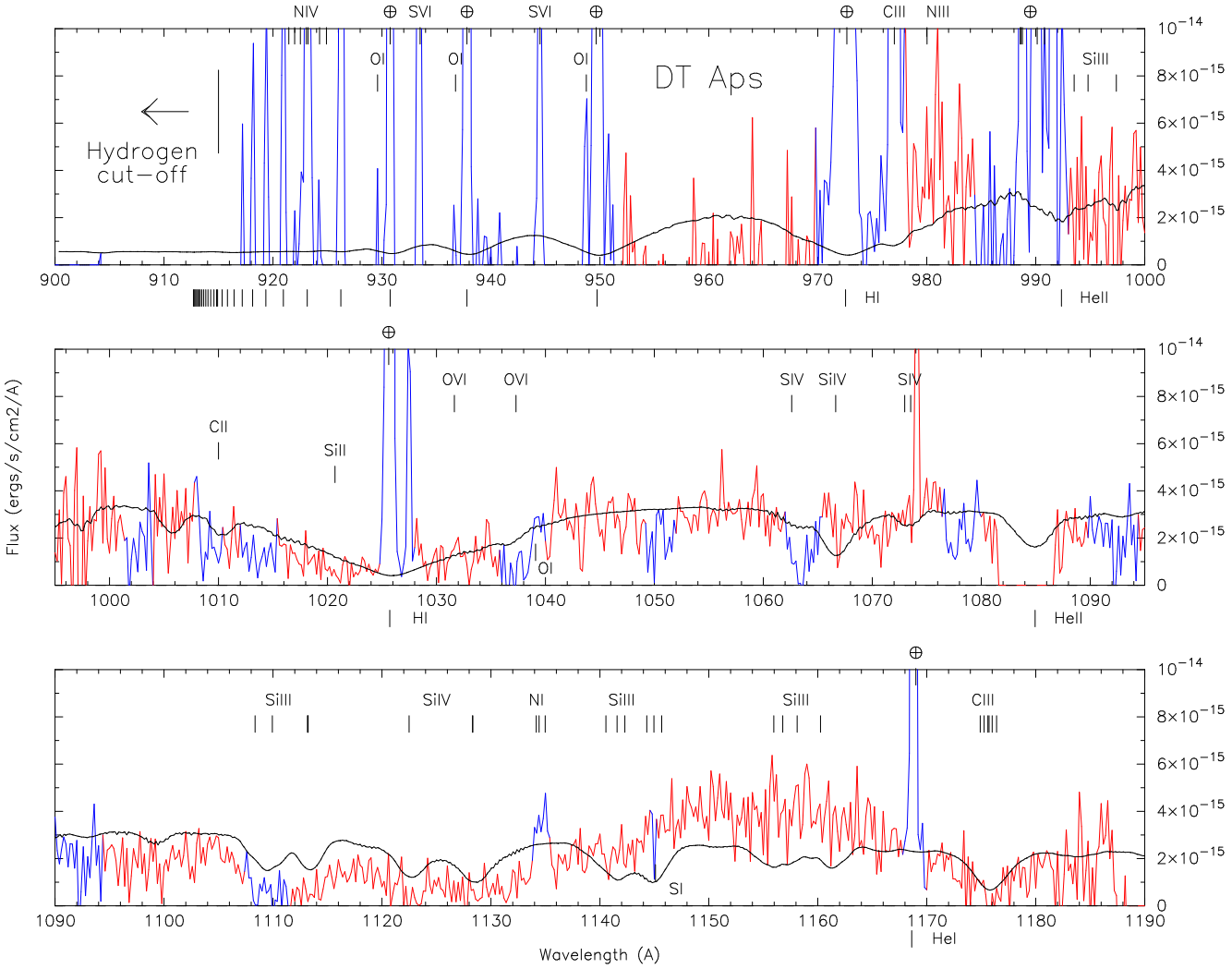

Fig. 6.— The best fit model (in black) to the *FUSE* spectrum (in red/light grey) of DT Aps. The regions that have been masked before fitting are in blue/dark grey (they consist mainly of ISM molecular hydrogen absorption lines and air glow emission). . The model consists of a WD with a mass $M = 0.8 M_{\odot}$, with T=37,000K, a silicon abundance of 10× solar, d=1700pc and $\chi^2 = 0.2050$. In order to fit the absorption lines profiles the projected rotational velocity $V_{rot} \sin i$ was set to 500km/s. Here we assumed $E(B-V) = 0.0$.

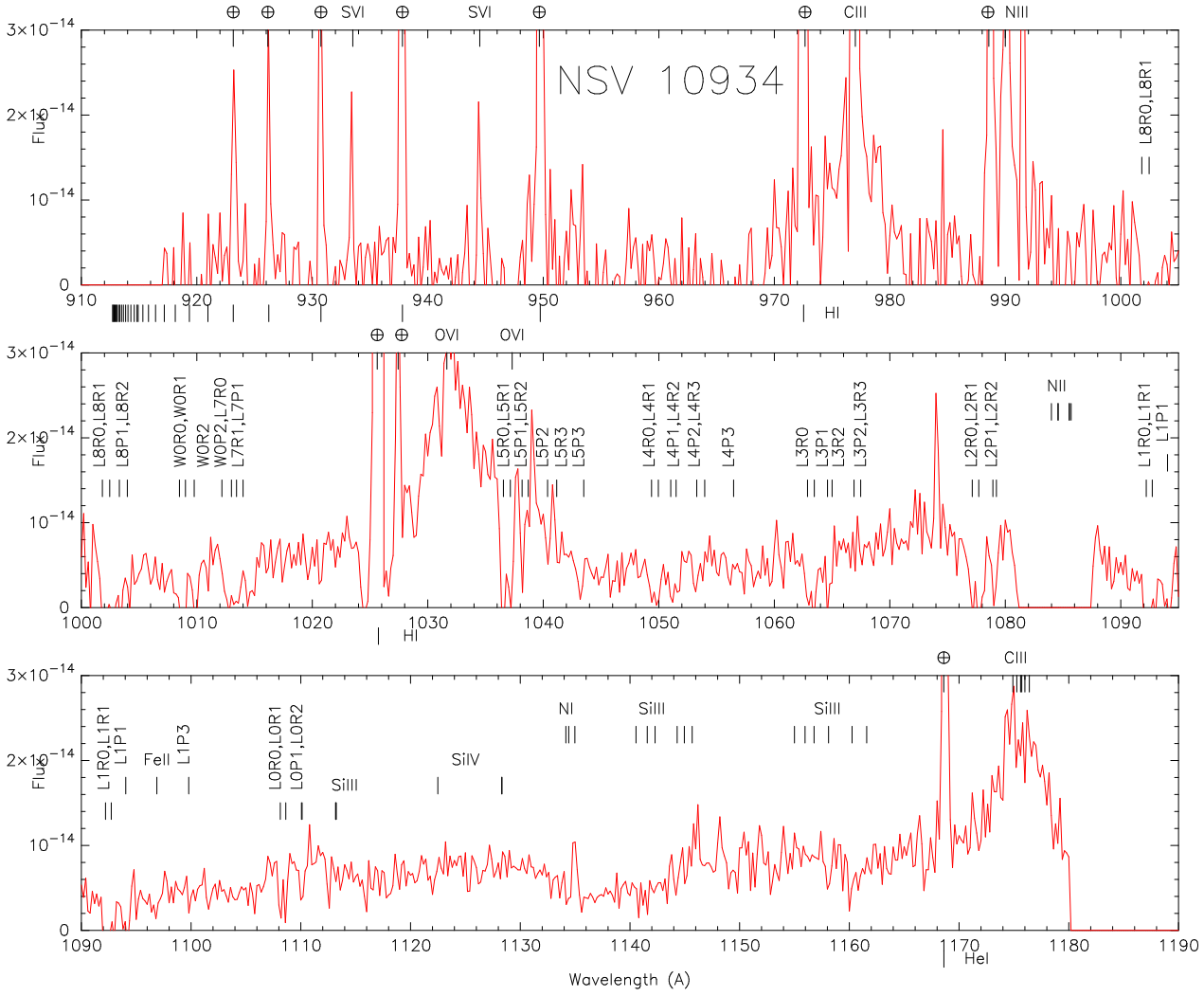

Fig. 7.— The *FUSE* spectrum of NSV 10934 has a low S/N especially in the shorter wavelengths due to the fact that the data from the 2bSiC, 2bLiF and 1aSiC channels were unusable and a large portion of the 1bLiF channel was lost to the worm. As a consequence there is gap around 1085Å. The continuum is rather flat with very broad emission lines from C III (λ977 & λ1175) and the O VI doublet. The Lyβ broad absorption feature is not detected, possibly due to the left wing of the very broad oxygen emission feature or to velocity broadening in a disk viewed at a high inclination. The ISM molecular lines are identified (labelled vertically). The metal lines have been marked but are not detected. All the sharp emission lines are due to air glow.

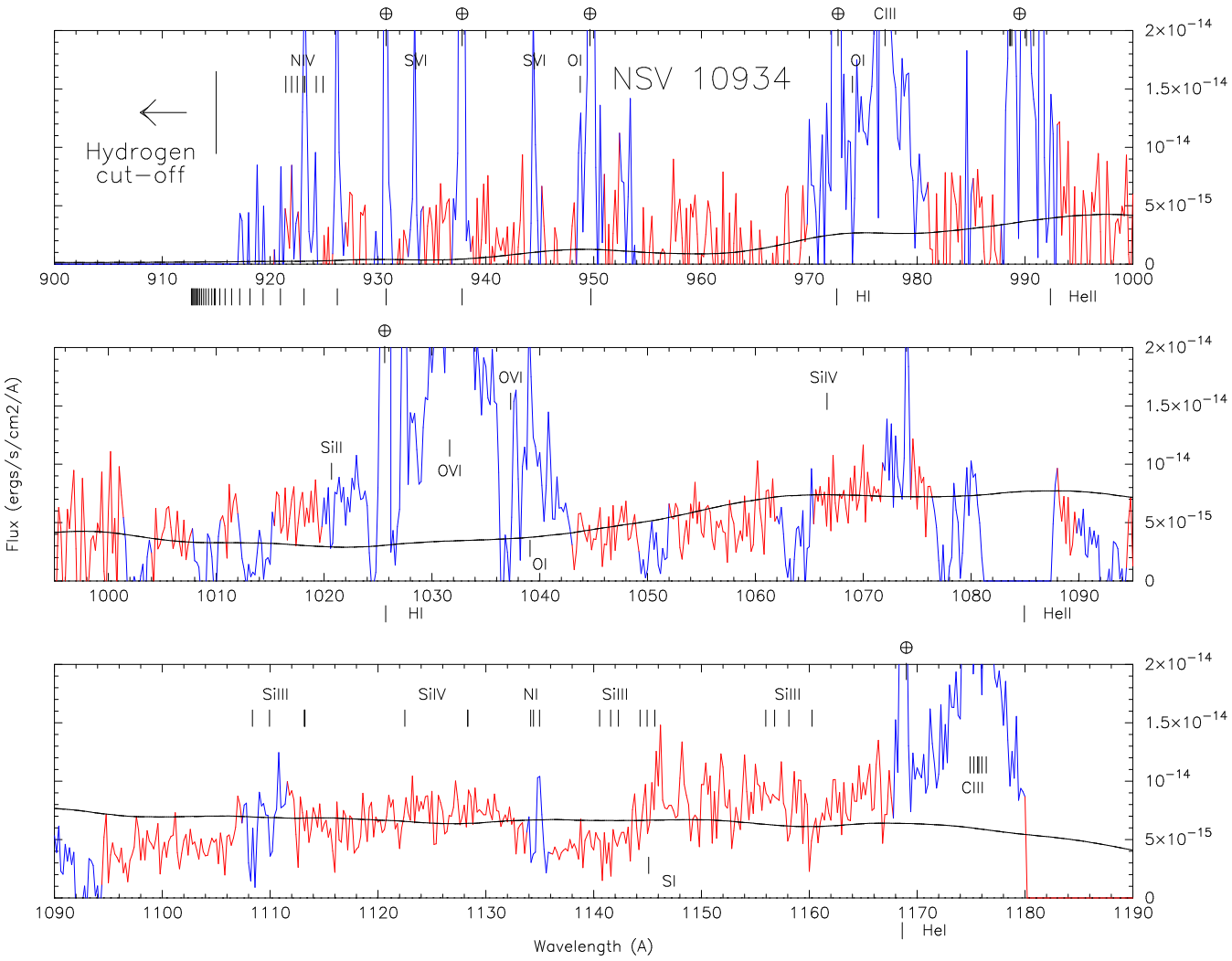

Fig. 8.— The best fit model to the *FUSE* spectrum of NSV 10934. The observed spectrum (in red/light gray) has been dereddened assuming E(B-V)=0.1. The regions that have been masked before modeling are shown in blue (dark gray). The best fit (in black) consists of a disk model with a $M = 1.2M_{wd}$, $\dot{M} = 10^{-10}$, and $i = 81°$, giving a distance of 187pc $\chi^2 = 0.146$.

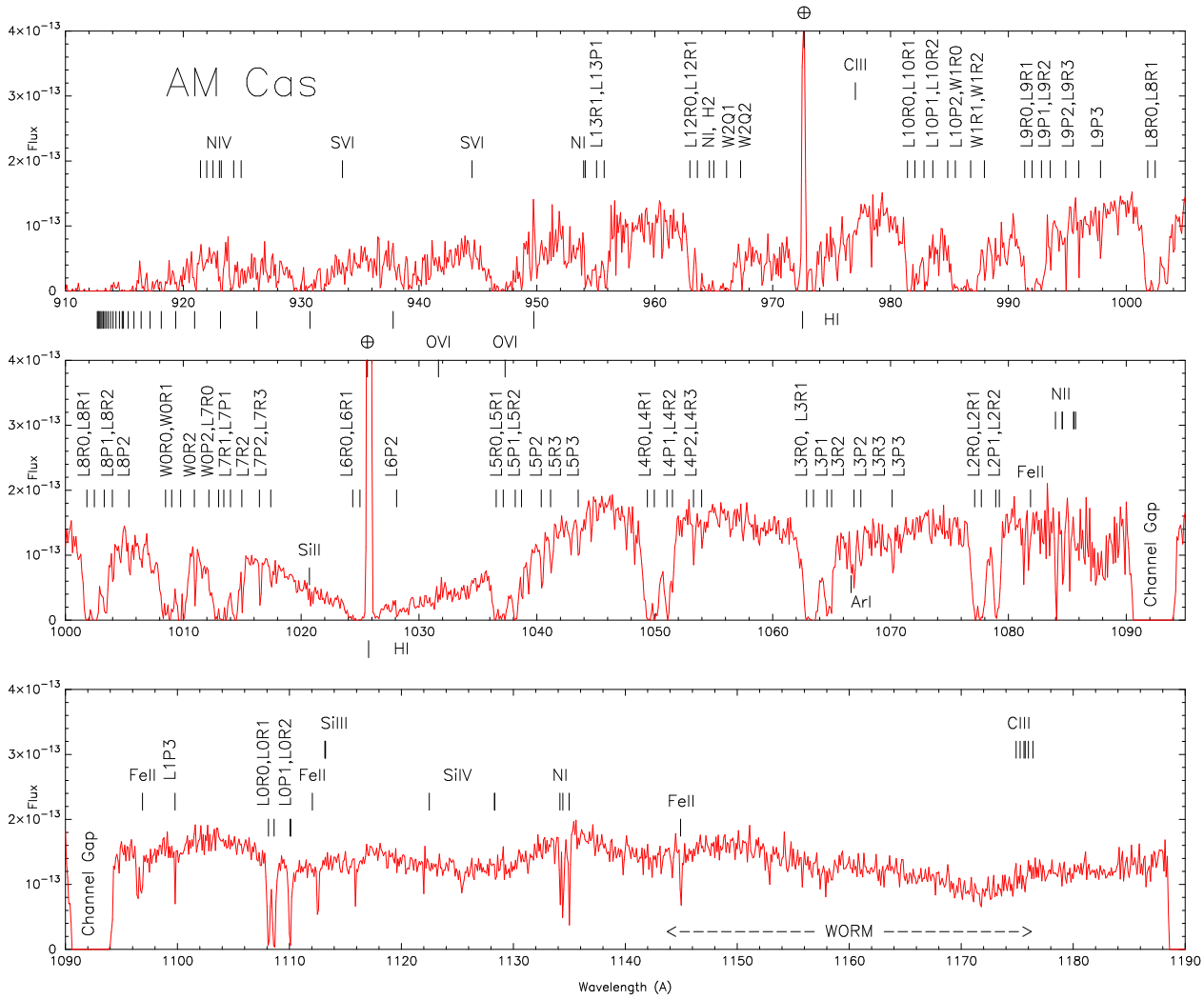

Fig. 9.— The *FUSE* spectrum of AM Cas with line identifications. The ISM molecular hydrogen absorption lines have been labeled vertically. This spectrum consists only of the 1-SiC and -LiF a & b channels, because of that there is a gap around 1095Å, and **the longer wavelengths are affected by the worm** (as shown). The higher ionization level metal lines are discussed in Fig.11 in the context of the fit model.

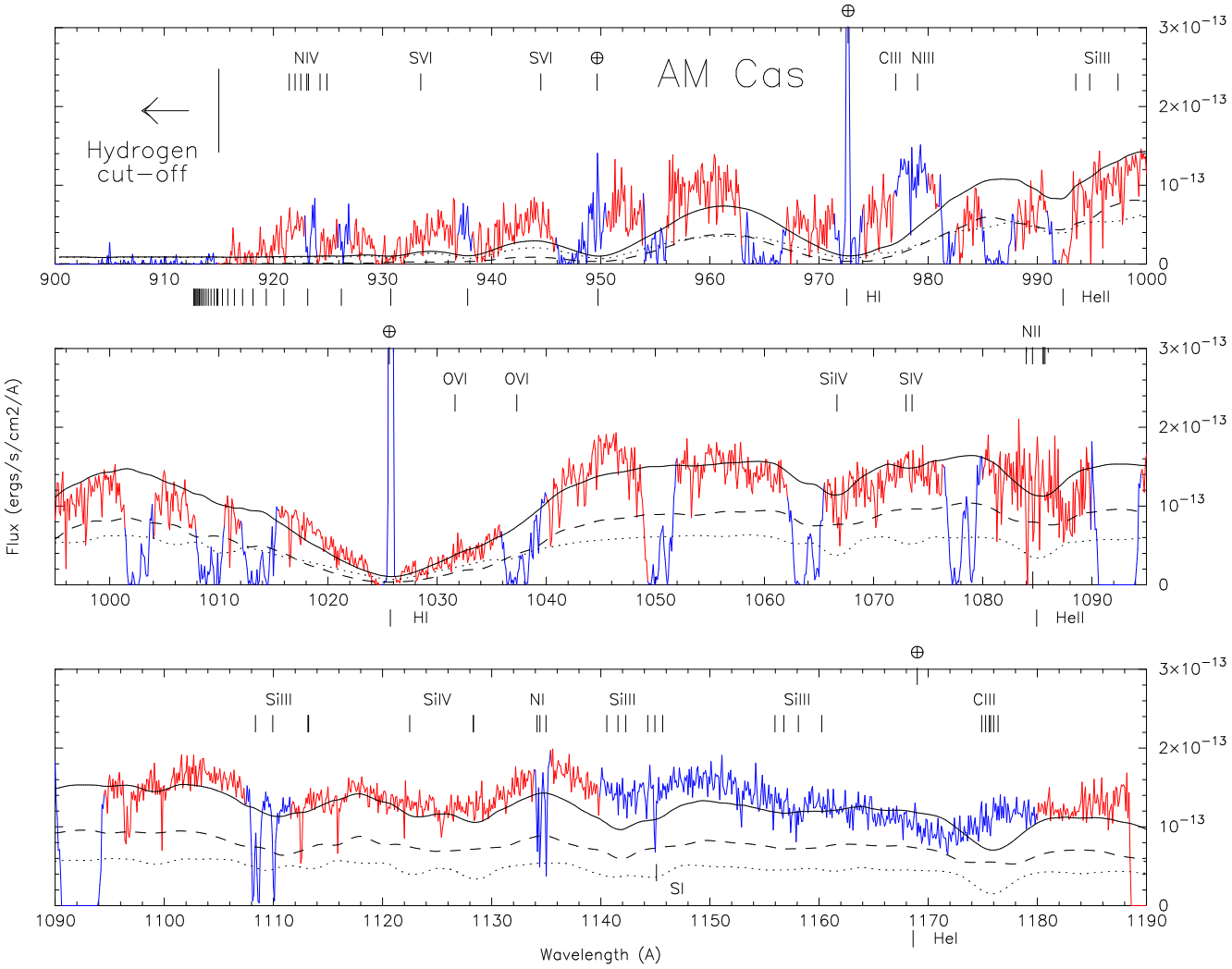

Fig. 10.— The best fit model (solid black line) to the *FUSE* spectrum of AM Cas (in light grey/red) assuming E(B-V)=0.0 is a WD+disk composite model. The regions that have been masked before fitting are shown in dark grey (blue). The WD model (dotted line) has $M = 0.8 M_{\odot}$, $T = 36,000$K, $V_{rot} \sin i$=500km/s, and the disk model (dashed-line) has a mass accretion rate $\dot{M} = 2{\times}10^{-10} M_{\odot}$/yr and an inclination $i = 18°$. This model gave a distance of 373pc, $\chi^2 = 0.563$, with the WD contributing 41% of the flux and the disk 59%.

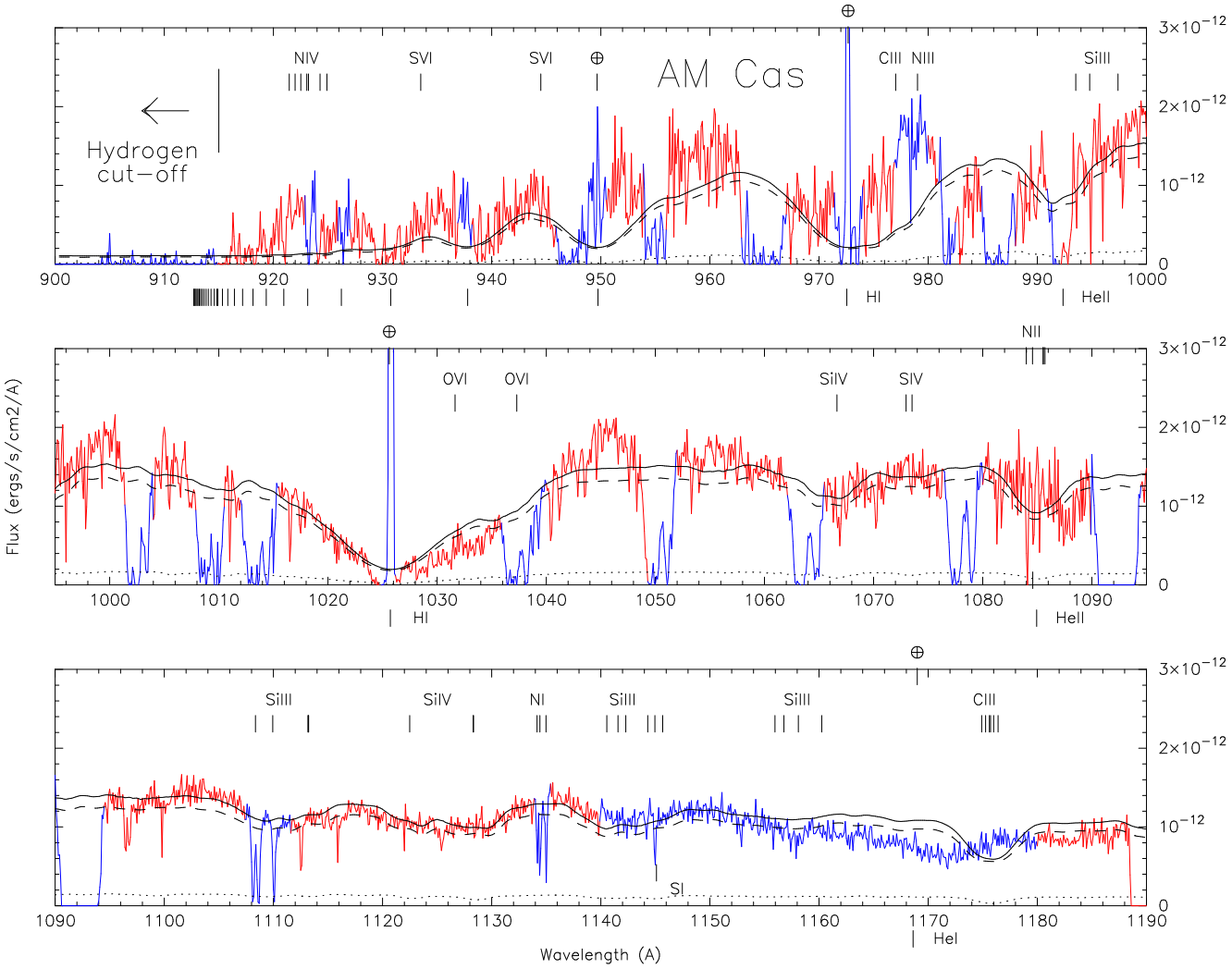

Fig. 11.— The best fit model (solid black) to the *FUSE* spectrum of AM Cas assuming E(B-V)=0.2 is a WD+disk composite model. The WD model (dotted line) has $M = 0.55 M_{\odot}$, $T = 35,000$K, $V_{rot} \sin i$=400km/s, and the disk model (dashed line) has a mass accretion rate $\dot{M} = 3 \times 10^{-9} M_{\odot}$/yr and an inclination $i = 18°$. This model gave a distance of 331pc, $\chi^2 = 0.538$, with the WD contributing 11% of the flux and the disk 89%. The excess flux in the shorter wavelengths could be due to emission from N IV and S VI. There seems to be some broad C III (977Å) & N III (980Å) emission, while the higher flux around ∼950-962Å cannot be accounted for. In the lower panel the Si III (1108-1113Å), Si IV (1123 & 1128Å), and Si III (1140-1145Å) lines are broadened (Keplerian motion) and are identified as the depression in the flux there. The Si III (∼1158Å) and C III (1175Å) are not identified, possibly due to the deterioration of the spectra in the region of the worm.

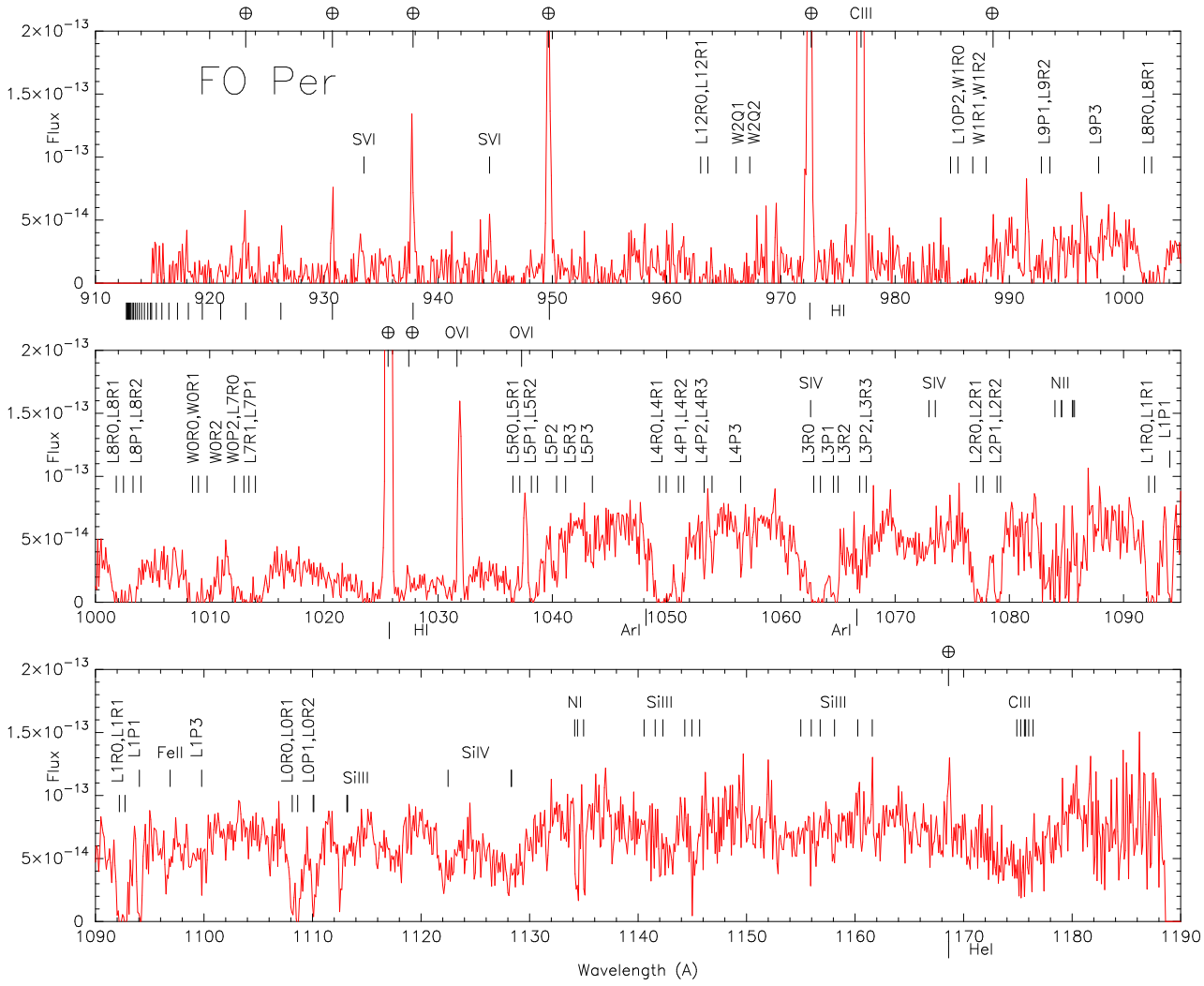

Fig. 12.— The *FUSE* spectrum of FO Per. All the sharp emission lines are due to geo- and helio-coronal contamination, including the S VI and O VI lines. All the ISM hydrogen molecular absorption lines have been annotated vertically. The broad Lyβ feature is visible, as well as broad carbon (C III 1175Å) and silicon (Si III 1113Å, Si IV 1123 & 1128Å, Si III ∼1140-1145Å) absorption features. All the other metal lines have not been identified, but have been marked for comparison.

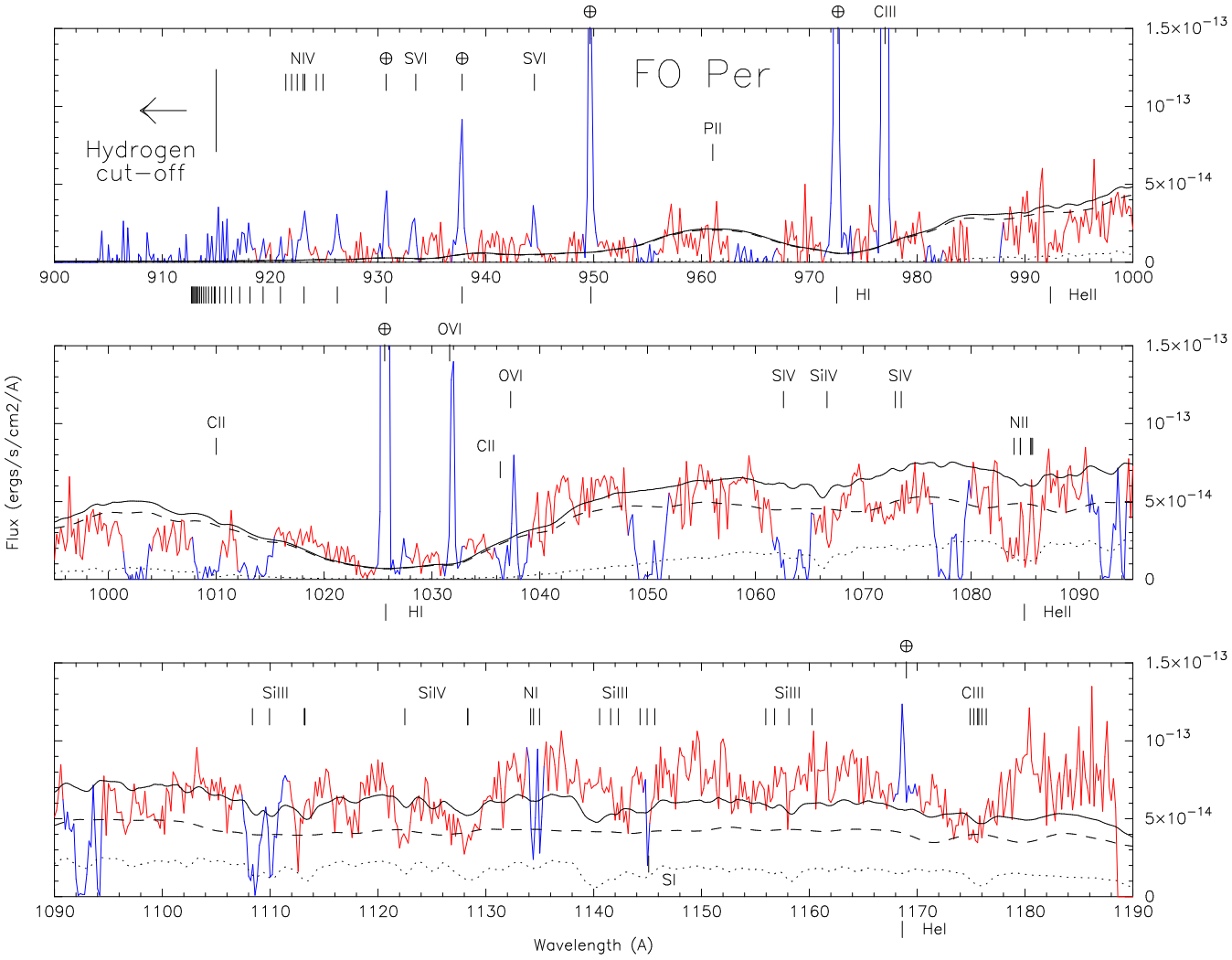

Fig. 13.— The best-fit WD+disk composite model (solid black) to the *FUSE* spectrum of FO Per assuming E(B-V)=0.0. The observed spectrum is in red (light gray) and the regions that have been masked for the fitting are in blue (dark gray). The WD model (dotted line) has $0.4M_{\odot}$, with $T_{wd} = 21,000$K, and $V_{rot} \sin i$ =200km/s, the disk model (dashed line) has $i = 75°$, and $\dot{M} = 10^{-8.5} M_{\odot} \mathrm{yr}^{-1}$. The distance obtained is d=291pc, and $\chi^2 = 0.258$. The WD contributes 29% of the FUV flux while the disk contributes 71%.

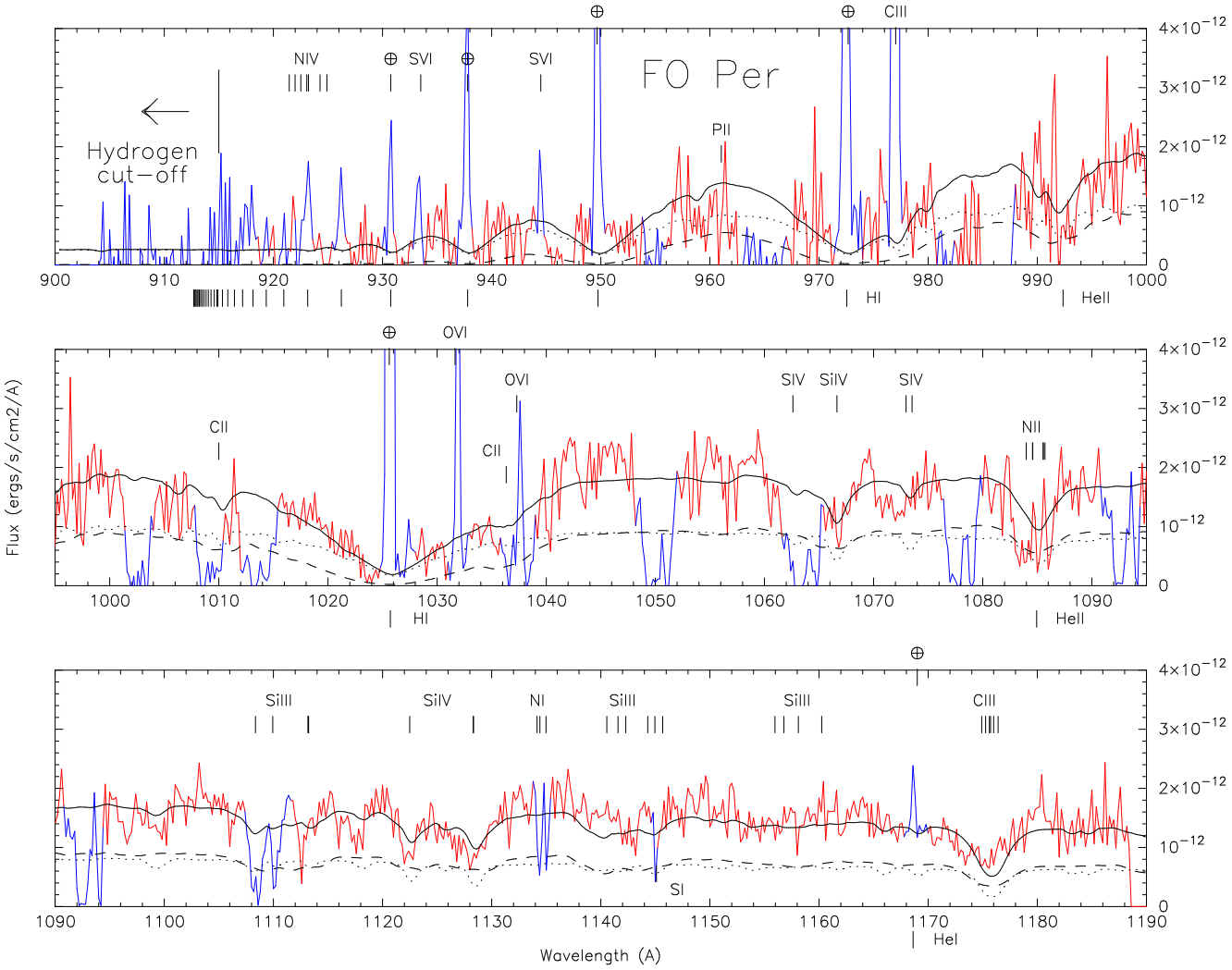

Fig. 14.— The best-fit WD+disk composite model to the dereddened *FUSE* spectrum of FO Per assuming E(B-V)=0.3. The WD model (dotted line) has a $0.4M_{\odot}$ and $T_{wd} = 40,000$K, and $V_{rot} \sin i$ =200km/s. The disk model (dashed line) has $i = 18°$, and $\dot{M} = 10^{-8.5} M_{\odot} \mathrm{yr}^{-1}$. The model gives a distance d=254pc with $\chi^2 = 0.146$. The WD contributes 52% of the FUV flux while the disk contributes 48%. When compared to the model, we find that the C III (1175Å) and Si IV (1123, 1128Å) lines are blue shifted by ∼2Å and ∼1Å respectively. The S IV (1063,1073Å) lines might also be blue-shifted.

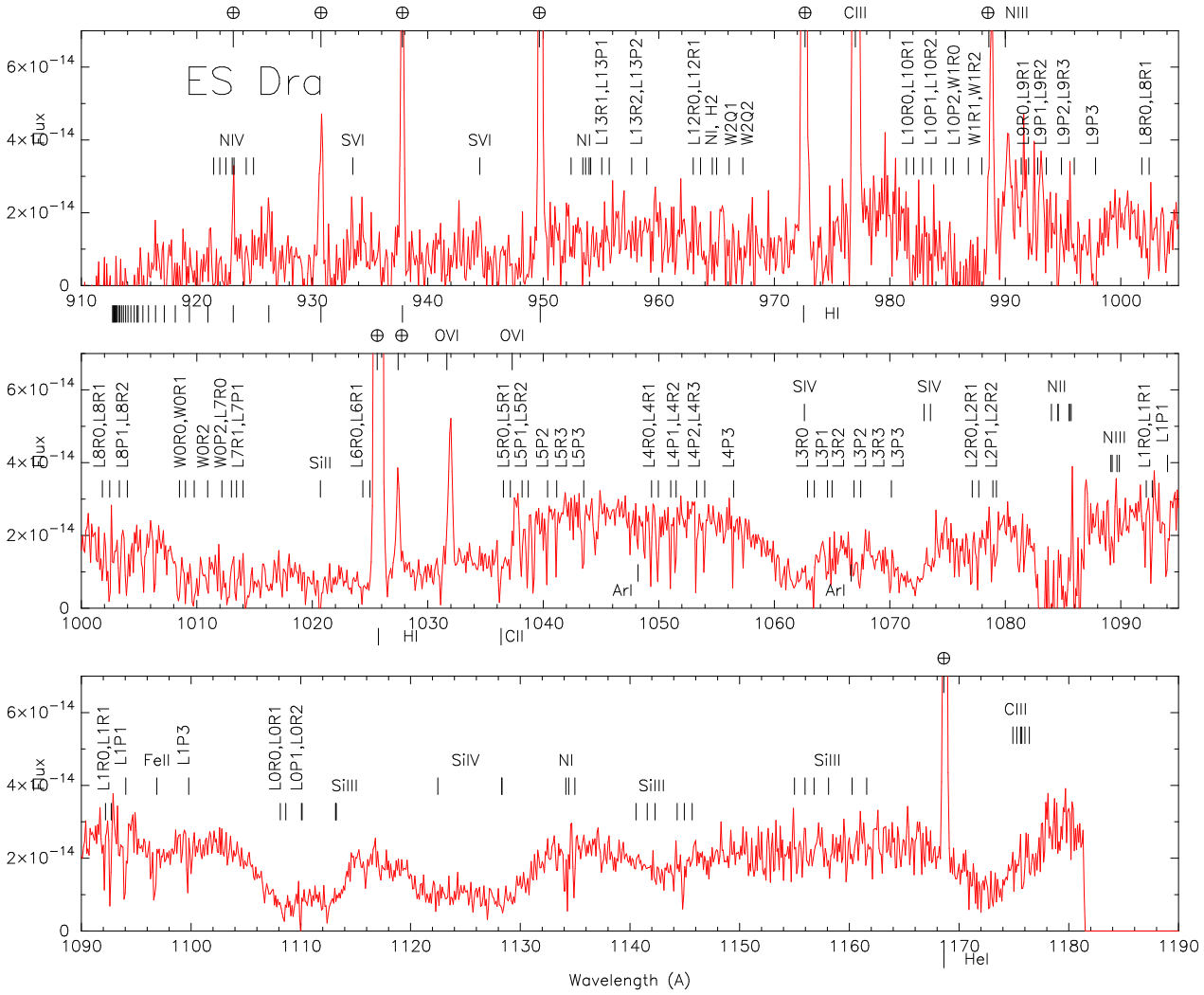

Fig. 15.— The *FUSE* spectrum of ES Dra with line identifications. All the sharp emission lines are due to geo- and helio-coronal contamination, including the S VI, O VI, and C III (977Å) lines. Broad absorption features from carbon and silicon are clearly seen, slightly blue-shifted. The shitfing of the lines is more apparent in Figs.16 & 17, where the observed spectrum is compared to the models.

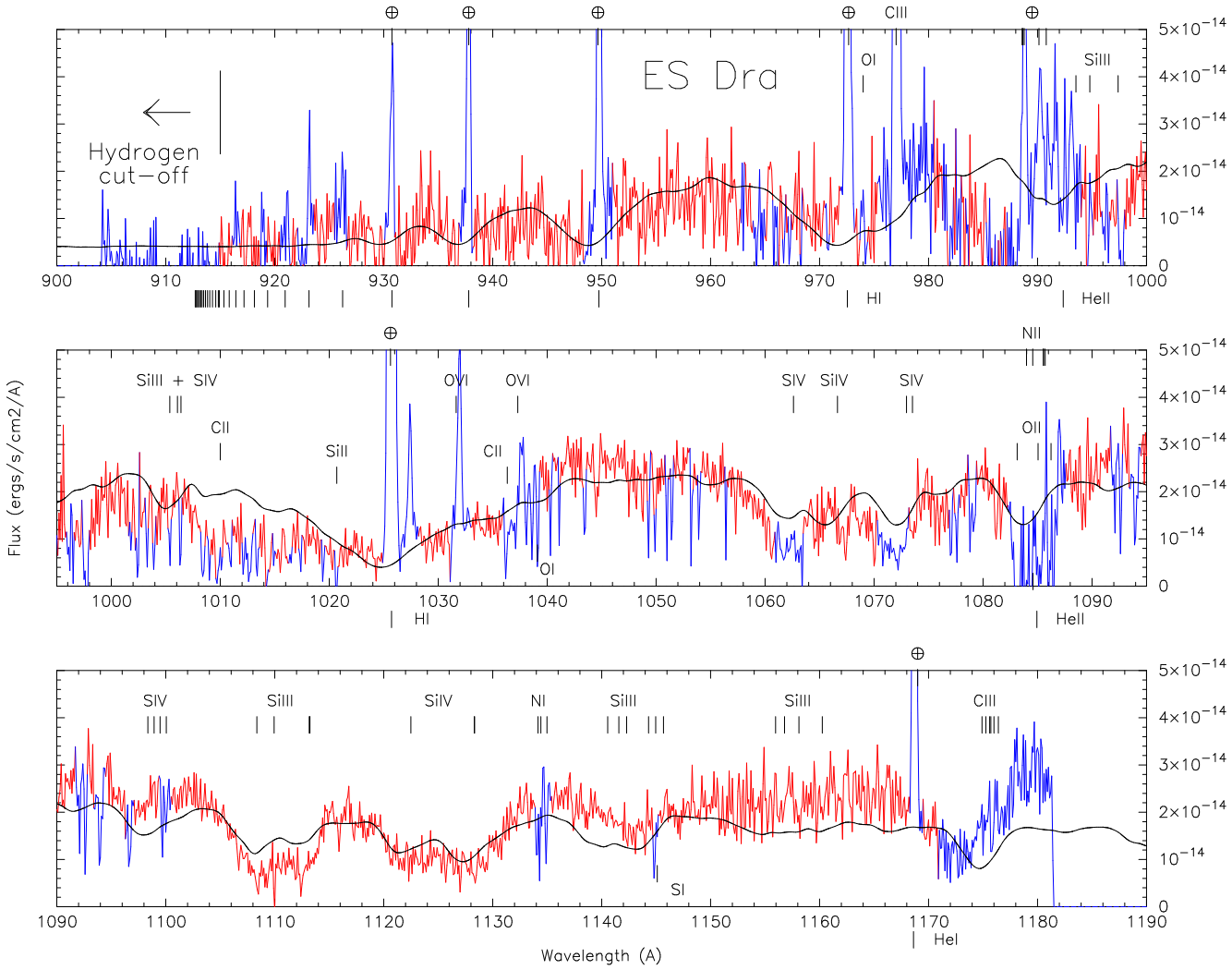

Fig. 16.— The best-fit accretion disk model to the *FUSE* spectrum of ES Dra. The regions of the spectrum that have been masked for the fitting are in blue. The disk model has a central accreting WD with a mass $M = 1.2M_{\odot}$, a mass accretion rate $\dot{M} = 10^{-9.5} M_{\odot}\mathrm{yr}^{-1}$, an inclination $i = 5°$, and gives a distance of 1754pc. We fine-tuned the fitting by setting the silicon and sulfur abundances 10× solar and 50× solar respectively, and we shifted the entire synthetic spectrum to the blue by 1.0Å. This resulted in $\chi^2 = 0.4280$.

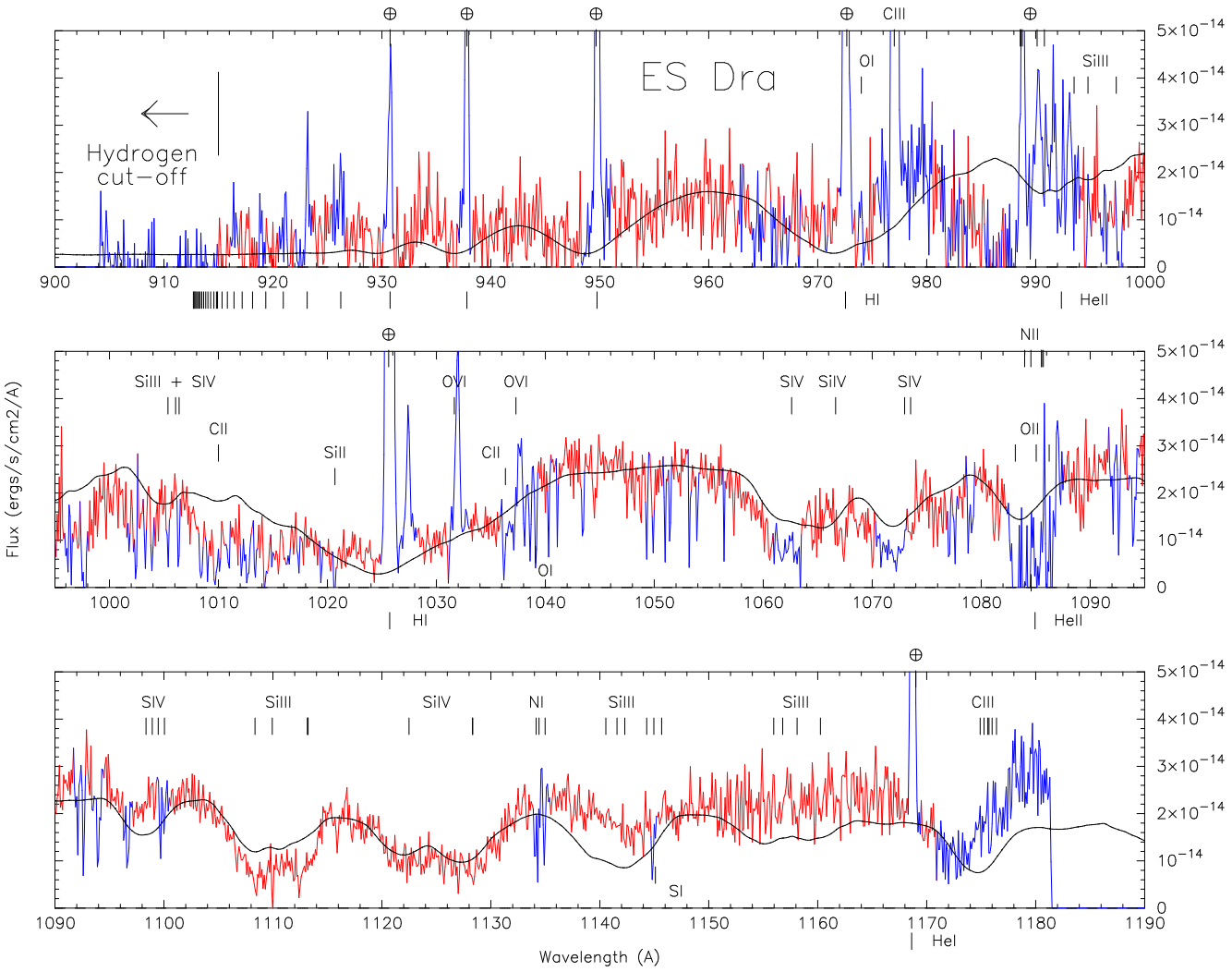

Fig. 17.— The best fit single component WD model to the *FUSE* spectrum of ES Dra. The WD has a temperature $T = 35,000$K, $log(g) = 7.8$ (corresponding to $M_{wd} \approx 0.58 M_{\odot}$), a projected rotational velocity $v_{rot} \sin i = 700$km/s, abundances $Si \approx 10\times$ solar, $S \approx 50\times$ solar and a blue-shift of 1.3Å. This model gives a distance of 773pc and $\chi^2 = 0.4277$. When compared to the synthetic spectrum, the observed spectrum clearly reveals the Si III (∼1110Å) and Si IV (1023 & 1028Å) lines; the Si III lines in the longer wavelenghts do not match the model The C III (1175Å) presents a P-Cygni profile; the S IV (1063, 1073, & 1099Å) lines are blue-shifted. The Si III + S IV (∼1006Å), C II (1010Å), Si IV (1066Å) lines are all contaminated with ISM absorption (see Fig.15 for comparison).

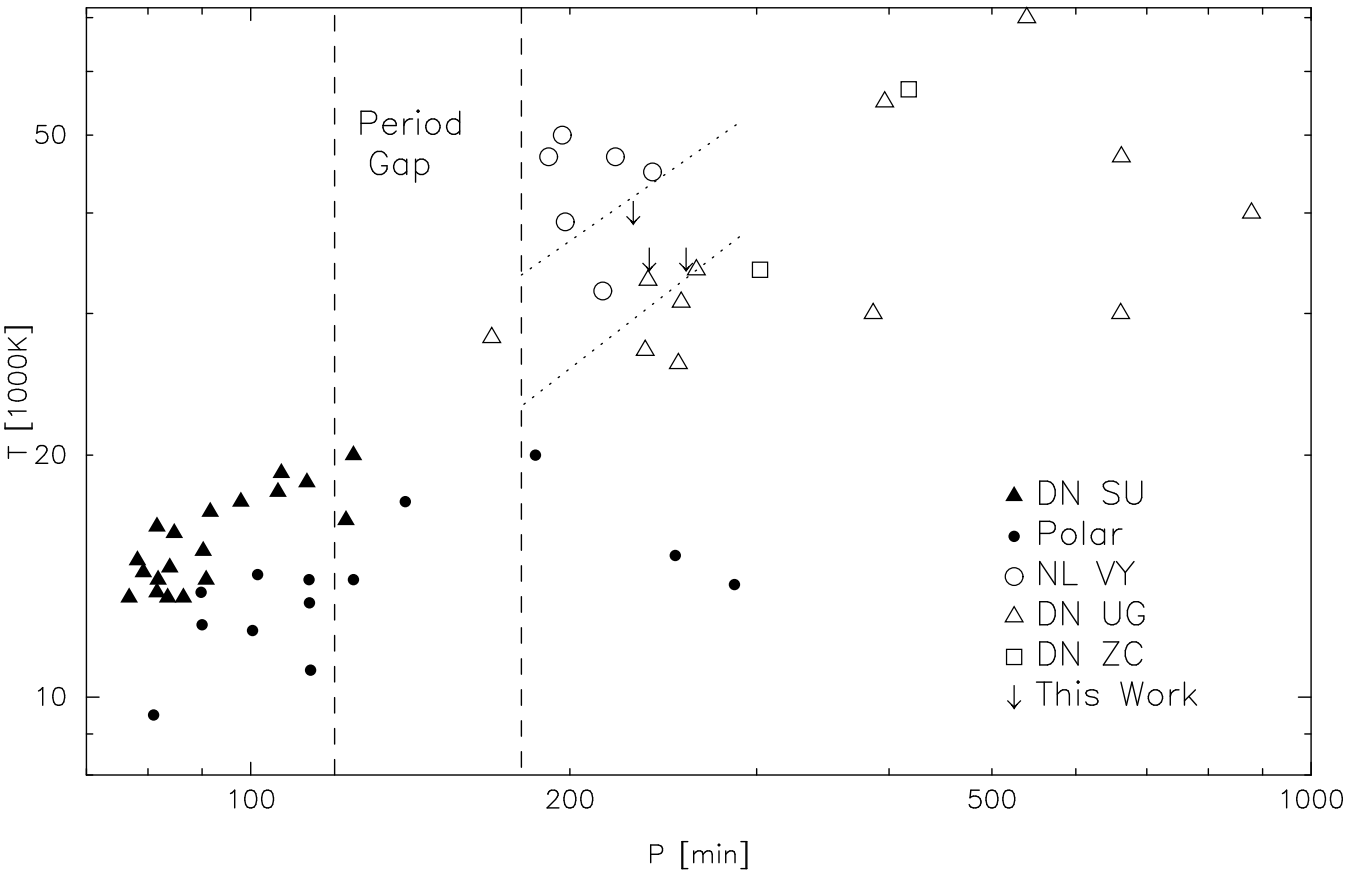

Fig. 18.— Effective White Dwarf Temperature as a function of the orbital period, from Table 5. There is a well defined separation between Polars and DN below the gap, and apparentlly also above the gap. There is clearly a lack of data points above the gap for Z Cam's, Polars and VY Scl's. There seems to be a separation in the $P - T_{eff}$ parameter space between Polars, SU UMa's, U Gem's and possibly VY Scl's. The 3 arrows (this work) are only upper limits and have been included here to show how important it is to obtain good FUV spectra and parallax for CVs in order to be able to derive robust results for the WD effective temperatures. The traditional magnetic braking above the period gap (Howell et al. 2001) is shown between the dotted lines.